Dark matter heats up in dwarf galaxies

Author(s):
Read, Justin I.; Walker, Matthew C.; Steger, Pascal

Publication date:
2019-03

Permanent link:
https://doi.org/10.3929/ethz-b-000336589

Originally published in:
Monthly Notices of the Royal Astronomical Society 484(1), https://doi.org/10.1093/mnras/sty3404

Funding acknowledgement:
128540 - Shedding light on dark matter (SNF)

Monthly Notices
of the
ROYAL ASTRONOMICAL SOCIETY

MNRAS **484,** 1401–1420 (2019)
Advance Access publication 2019 January 3

doi:10.1093/mnras/sty3404

Dark matter heats up in dwarf galaxies

J. I. Read [1]★ M. G. Walker [2] and P. Steger[3]

[1]*Department of Physics, University of Surrey, Guildford GU2 7XH, UK*
[2]*McWilliams Center for Cosmology, Department of Physics, Carnegie Mellon University, 5000 Forbes Ave., Pittsburgh, PA 15213, USA*
[3]*Institute for Astronomy, Department of Physics, ETH Zürich, Wolfgang-Pauli-Strasse 27, CH-8093 Zürich, Switzerland*

Accepted 2018 December 10. Received 2018 November 29; in original form 2018 August 21

ABSTRACT

Gravitational potential fluctuations driven by bursty star formation can kinematically 'heat up' dark matter at the centres of dwarf galaxies. A key prediction of such models is that, at a fixed dark matter halo mass, dwarfs with a higher stellar mass will have a lower central dark matter density. We use stellar kinematics and HI gas rotation curves to infer the inner dark matter densities of eight dwarf spheroidal and eight dwarf irregular galaxies with a wide range of star formation histories. For all galaxies, we estimate the dark matter density at a common radius of 150 pc, $\rho_{\rm DM}(150\,{\rm pc})$. We find that our sample of dwarfs falls into two distinct classes. Those that stopped forming stars over 6 Gyr ago favour central densities $\rho_{\rm DM}(150\,{\rm pc}) > 10^8\,{\rm M}_\odot\,{\rm kpc}^{-3}$, consistent with cold dark matter cusps, while those with more extended star formation favour $\rho_{\rm DM}(150\,{\rm pc}) < 10^8\,{\rm M}_\odot\,{\rm kpc}^{-3}$, consistent with shallower dark matter cores. Using abundance matching to infer pre-infall halo masses, M_{200}, we show that this dichotomy is in excellent agreement with models in which dark matter is heated up by bursty star formation. In particular, we find that $\rho_{\rm DM}(150\,{\rm pc})$ steadily decreases with increasing stellar mass-to-halo mass ratio, M_*/M_{200}. Our results suggest that, to leading order, dark matter is a cold, collisionless, fluid that can be kinematically 'heated up' and moved around.

Key words: galaxies: dwarf – galaxies: haloes – galaxies: kinematics and dynamics – galaxies: star formation – cosmology: observations – dark matter.

1 INTRODUCTION

The standard Λ cold dark matter (ΛCDM) cosmological model gives a remarkable description of the growth of structure in the Universe on large scales (e.g. Clowe et al. 2006; Springel, Frenk & White 2006; Dawson et al. 2013; Planck Collaboration et al. 2014; Baur et al. 2016; Wang et al. 2016). Yet, on smaller scales inside the dark matter (DM) haloes of galaxies, there have been long-standing tensions (e.g. Bullock & Boylan-Kolchin 2017). The oldest of these is the 'cusp–core' problem. Pure DM structure formation simulations in ΛCDM predict a universal DM halo profile that has a dense 'cusp' at the centre, with inner density $\rho_{\rm DM} \propto r^{-1}$ (Dubinski & Carlberg 1991; Navarro, Frenk & White 1996b). By contrast, observations of gas-rich dwarf galaxy rotation curves have long favoured DM 'cores', with $\rho_{\rm DM} \sim$ constant (Flores & Primack 1994; Moore 1994; de Blok 2010; Read et al. 2017).

The cusp–core problem has generated substantial interest over the past two decades because it may point to physics beyond the collisionless 'CDM' typically assumed to date. Spergel & Steinhardt (2000) were the first to suggest that 'self-interacting dark matter' (SIDM) – that invokes a new force acting purely in the dark sector – could transform a dense cusp to a core through energy transfer between the DM particles (e.g. Rocha et al. 2013; Elbert et al. 2015; Kaplinghat, Tulin & Yu 2016; Robles et al. 2017; Schneider et al. 2017). Warm dark matter has also been proposed as a solution to the cusp–core problem (e.g. Hogan & Dalcanton 2000; Avila-Reese et al. 2001; Bode, Ostriker & Turok 2001; Lovell et al. 2014; Schneider et al. 2017, but see Dalcanton & Hogan 2001; Macciò et al. 2012 and Shao et al. 2013). Other solutions include 'fuzzy DM' (Hu, Barkana & Gruzinov 2000; Hui et al. 2017), 'fluid' DM (Peebles 2000), and 'wave-like' DM (Schive, Chiueh & Broadhurst 2014).

However, there is a more prosaic explanation for the cusp–core problem. If gas is slowly accreted on to a dwarf galaxy and then suddenly removed (for example by stellar winds or supernovae feedback) this causes the DM halo to expand, irreversibly lowering its central density[1] (Navarro, Eke & Frenk 1996a). Gnedin & Zhao

[1]Note that there is an alternative mechanism by which stars and gas can alter the inner DM density profile. El-Zant, Shlosman & Hoffman (2001) were the first to suggest that dense gas clumps could impart angular momentum to the inner DM density profile by dynamical friction, causing a cusp to flatten to a core (see also Del Popolo 2009; Goerdt et al. 2010; Cole, Dehnen &

★ E-mail: justin.inglis.read@gmail.com

(2002) showed that, for reasonable gas fractions and collapse factors, the overall effect of this 'DM heating' is small. However, if the effect repeats over several cycles of star formation, it accumulates, leading eventually to complete DM core formation (Read & Gilmore 2005). Indeed, recent numerical simulations of dwarf galaxies that resolve the impact of individual supernovae on the interstellar medium find that the gas mass within the projected half-light radius of the stars, $R_{1/2}$, naturally rises and falls on a time-scale comparable to the local dynamical time,[2] transforming an initial DM cusp to a core (e.g. Mashchenko, Wadsley & Couchman 2008; Pontzen & Governato 2012; Oñorbe et al. 2015; Read et al. 2016a; Tollet et al. 2016, and for a review see Pontzen & Governato 2014). Such simulations have already made several testable predictions. Teyssier et al. (2013) show that the gas flows that transform DM cusps to cores lead to a bursty star formation history (SFH), with a peak-to-trough ratio of 5−10 and a duty cycle comparable to the local dynamical time. Furthermore, the stars are dynamically 'heated' similarly to the DM, leading to a stellar velocity dispersion that approaches the local rotational velocity of the stars ($v/\sigma \sim 1$) inside $R_{1/2}$. Both of these predictions are supported by observations of dwarf galaxies (e.g. Dohm-Palmer et al. 1998, 2002; Young et al. 2007; Leaman et al. 2012; Kauffmann 2014; Sparre et al. 2017; Wheeler et al. 2017). Further evidences for 'DM heating' come from the observed age gradients in dwarfs (El-Badry et al. 2016).

While there is strong evidence that dwarf galaxies have bursty SFHs, this is only circumstantial evidence for DM heating. The real 'smoking gun' for DM cusp–core transformations lies in another key prediction from recent numerical models: DM core formation requires several cycles of gas inflow and outflow (Read & Gilmore 2005; Pontzen & Governato 2012). Thus, at fixed halo mass, galaxies that have formed more stars (i.e. that have undergone more gas inflow–outflow cycles) will have a lower central DM density (Pontzen & Governato 2012; Peñarrubia et al. 2012; Di Cintio et al. 2014a; Brook & Di Cintio 2015; Oñorbe et al. 2015; Read et al. 2016a; Di Cintio et al. 2017; Bermejo-Climent et al. 2018). By contrast, solutions to the cusp–core problem that invoke exotic DM predict no relationship between the central DM densities of dwarfs and their SFHs.[3]

Whether or not a dwarf will form a DM core depends primarily on the number and amplitude of gas inflow–outflow cycles, and on the amount of DM that needs to be evacuated from the centre of the dwarf to form the core. This can be posed in the form of an energy argument, whereby the total energy available to move gas around depends on the total stellar mass formed, M_*, while the energy required to unbind the DM cusp depends on the DM halo mass, M_{200} (Peñarrubia et al. 2012). Thus, whether or not a DM core will form in a given dwarf galaxy depends primarily on its stellar mass to halo mass *ratio*, M_*/M_{200} (Di Cintio et al. 2014a). However, since M_{200} is challenging to extrapolate from the data, in this paper we consider also a proxy for the ratio M_*/M_{200}: the star formation 'truncation time', $t_{\rm trunc}$. We define this to be the time when the dwarf's star formation rate (SFR) fell by a factor of 2 from its peak value.[4] This can be used as a proxy for M_*/M_{200} so long as the SFR is approximately constant[5] (as is the case for the sample of dwarfs that we consider in this paper; see Read & Erkal 2018 and Section 4). In this case, dwarfs with $t_{\rm trunc} \rightarrow 0$ Gyr have $M_*/M_{200} \rightarrow 0$, while those with $t_{\rm trunc} \rightarrow 13.8$ Gyr (i.e. the age of the Universe) have formed stars for as long as possible and have, therefore, maximized both M_*/M_{200} and their ability to produce a DM core. Unlike M_{200}, however, $t_{\rm trunc}$ has the advantage that it is readily estimated from the dwarf's SFH (see Section 4).

In this paper, we set out to test the above key prediction of DM heating models, that dwarfs with 'extended star formation' (i.e. $t_{\rm trunc} \rightarrow 13.8$ Gyr and maximal M_*/M_{200}) have DM cores, while those with 'truncated star formation' (i.e. $t_{\rm trunc} \rightarrow 0$ Gyr and minimal M_*/M_{200}) have DM cusps. To achieve this, we estimate the central DM density, M_*, $t_{\rm trunc}$, and M_{200} for a sample of nearby dwarf galaxies with a wide range of SFHs. Our sample includes gas-poor dwarf spheroidal galaxies (dSphs) whose star formation ceased shortly after the beginning of the Universe, dSphs with extended star formation that shut down only very recently, and gas-rich dwarf irregular galaxies (dIrrs) that are still forming stars today. This requires us to accurately infer the DM distribution in both gas-rich and gas-poor galaxies. For the former, we use HI rotation curves as in Read et al. (2017); for the latter, we use line-of-sight stellar kinematics. However, with only line-of-sight velocities, there is a well-known degeneracy between the radial density profile (that we would like to measure) and the velocity anisotropy of the dwarf (see Section 3.1 and Binney & Mamon 1982; Merrifield & Kent 1990; Battaglia, Helmi & Breddels 2013; Read & Steger 2017). In Read & Steger (2017) and Read, Walker & Steger (2018), we introduced a new mass modelling tool – GravSphere – that breaks this degeneracy by using 'virial shape parameters' (VSPs). We used a large suite of mock data to demonstrate that with ∼500 radial velocities, GravSphere is able to correctly infer the DM density profile over the radial range $0.5 < r/R_{1/2} < 2$, within its 95 per cent confidence intervals. Here, we use GravSphere to infer the inner DM density of eight Milky Way dSphs that have radial velocities for $\gtrsim 190$ member stars. We emphasize that, while with of order 500 radial velocities, GravSphere is not able to obtain a robust inference of the inner *slope* of the DM density profile, it can constrain the *amplitude* of the inner DM density at ∼150 pc (Read

Wilkinson 2011 for more recent work on this). Such a mechanism still requires stellar feedback to then destroy these dense gas clumps. Otherwise, the inner stellar density that results would be too high to be consistent with observations (e.g. Nipoti & Binney 2015). The predictions from this class of model can be rather degenerate with 'DM heating' due to potential fluctuations (Del Popolo & Pace 2016) and it may well be that both act in tandem in dwarf galaxies. This remains an area of active research.

[2]Fluctuations in the central gas mass need not be very large to excite DM heating, so long as they are repeated enough times. Read, Agertz & Collins (2016a) find in their simulations that the dynamical mass within $R_{1/2}$ fluctuates by just ∼10 per cent, yet this is sufficient transform a DM cusp to a core within $R_{1/2}$.

[3]Most exotic DM models designed to solve the cusp–core problem predict that *all* dwarfs should have a central DM core. However, there can be exceptions to this. In SIDM models with a high self-interaction cross-section, for example, DM haloes undergo 'core collapse', increasing their central density at late times (e.g. Vogelsberger, Zavala & Loeb 2012). However, while this will lead to some stochasticity in the central DM density of dwarfs, it will not lead to any relationship between their central DM densities and their SFHs.

[4]This is similar to the concept of 'fast' and 'slow' dwarfs introduced by Gallart et al. (2015) and explored in more detail by Bermejo-Climent et al. (2018). However, our definition here is more readily applied to our sample of both dSphs and dIrrs (see also Read & Erkal (2018) for a discussion on this point.

[5]If dwarfs have significant gaps in their SFHs, then this correspondence between $t_{\rm trunc}$ and M_*/M_{200} can break (e.g. Wright et al. 2019). For this reason, in this paper, we will look for anticorrelations between the central DM density of dwarfs and $t_{\rm trunc}$ (that is easier to measure) and M_*/M_{200} (that is more fundamental, but harder to estimate).

et al. 2018). As we shall show, this is sufficient to test DM heating models.

This paper is organized as follows. In Section 2, we briefly review the cusp–core problem in ΛCDM, and we explain why a robust estimate of the amplitude of the DM density at 150 pc is sufficient for testing DM heating models. In Section 3, we describe our method for measuring the DM density profile from stellar kinematics (GravSphere; Section 3.1) and HI rotation curves (Section 3.2). In Section 4, we describe our data compilation for our sample of dIrrs and dSphs, including their SFHs and estimates of M_{200} taken from the literature. In Section 5, we present our key results. In Section 6, we compare our measurements with previous work in the literature. We discuss the robustness of our results and their implications for 'DM heating' and the nature of DM. Finally, in Section 7 we present our conclusions.

2 THE CUSP–CORE PROBLEM IN ΛCDM

In this section, we briefly review the cusp–core problem in ΛCDM. This broadly follows a similar review presented in Read et al. (2018); however, we reproduce this here in order to introduce some key equations that we will need later on, and for this paper to be self-contained.

Pure DM structure formation simulations in ΛCDM predict DM haloes that have a 'Navarro, Frenk and White' (NFW) density profile (Navarro et al. 1996b):

$$\rho_{\rm NFW}(r) = \rho_0 \left(\frac{r}{r_{\rm s}}\right)^{-1} \left(1+\frac{r}{r_{\rm s}}\right)^{-2} \quad (1)$$

where the central density ρ_0 and scale length $r_{\rm s}$ are given by:

$$\rho_0 = \rho_{\rm crit}\Delta c_{200}^3 g_{\rm c}/3; \quad r_{\rm s} = r_{200}/c_{200} \quad (2)$$

$$g_{\rm c} = \frac{1}{\log(1+c_{200}) - \frac{c_{200}}{1+c_{200}}} \quad (3)$$

and:

$$r_{200} = \left[\frac{3}{4} M_{200} \frac{1}{\pi\Delta\rho_{\rm crit}}\right]^{1/3} \quad (4)$$

where c_{200} is the concentration parameter; $\Delta = 200$ is the overdensity parameter; $\rho_{\rm crit} = 136.05\,{\rm M}_\odot\,{\rm kpc}^{-3}$ is the critical density of the Universe at redshift $z = 0$; r_{200} is the virial radius; and M_{200} is the virial mass.

The mass and concentration of haloes in ΛCDM are correlated (e.g. Dutton & Macciò 2014):

$$\log_{10}(c_{200}) = 0.905 - 0.101\log_{10}(M_{200}h - 12) \quad (5)$$

with scatter $\Delta\log_{10}(c_{200}) = 0.1$, where $h \sim 0.7$ is the Hubble parameter.

Recent simulations, that have sufficient spatial resolution to capture the dense multiphase interstellar medium ($\Delta x \lesssim 100$ pc), and that include the effects of gas cooling, star formation, and feedback, find that DM cusps are transformed to cores in the centres of dwarf galaxies (e.g. Mashchenko et al. 2008; Pontzen & Governato 2012; Teyssier et al. 2013; Di Cintio et al. 2014a; Pontzen & Governato 2014; Oñorbe et al. 2015; Read et al. 2016a). Read et al. (2016a) introduced a fitting function to parametrize this cusp–core transformation, the 'coreNFW' profile. This has a cumulative mass profile given by:

$$M_{\rm cNFW}(<r) = M_{\rm NFW}(<r) f^n \quad (6)$$

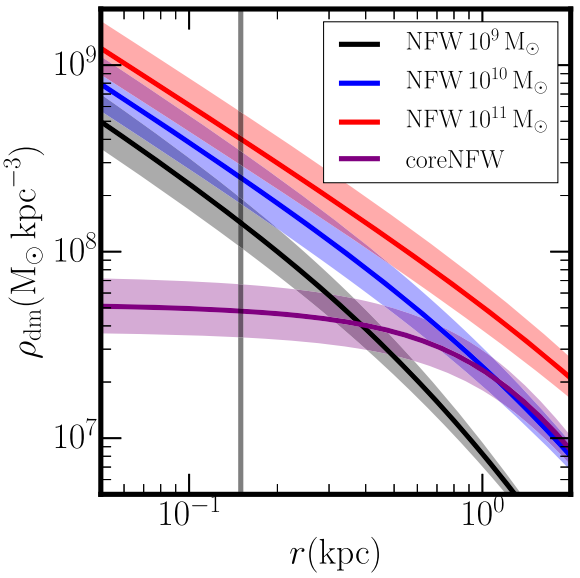

Figure 1. DM density profiles in ΛCDM. The black, blue, and red lines show results from fits to pure DM structure formation simulations (i.e. NFW profiles; equation 1) for three halo masses: $M_{200} = 10^9$, 10^{10}, and 10^{11} M$_\odot$, as marked in the legend. The purple line shows a fit to a model in which star formation 'heats up' the DM halo, lowering its central density (i.e. a coreNFW profile; equation 9). The median lines assume that haloes lie on the $M_{200} - c_{200}$ relation (equation 5), while the shaded regions show the 1σ scatter in this relation. Notice that the central densities of the cusped (black, blue, and red) and cored (purple) models is very different. A single measurement of the density at 150 pc (vertical grey line) is sufficient to differentiate the models, independently of the halo mass.

where $M_{\rm NFW}(<r)$ is the NFW cumulative mass profile:

$$M_{\rm NFW}(r) = M_{200} g_{\rm c} \left[\ln\left(1+\frac{r}{r_{\rm s}}\right) - \frac{r}{r_{\rm s}}\left(1+\frac{r}{r_{\rm s}}\right)^{-1}\right] \quad (7)$$

and f^n generates a shallower density profile at radii $r \lesssim r_{\rm c}$:

$$f^n = \left[\tanh\left(\frac{r}{r_{\rm c}}\right)\right]^n \quad (8)$$

The density profile of the coreNFW model is given by:

$$\rho_{\rm cNFW}(r) = f^n \rho_{\rm NFW} + \frac{n f^{n-1}(1-f^2)}{4\pi r^2 r_{\rm c}} M_{\rm NFW} \quad (9)$$

(The other main fitting function proposed in the literature to date – the Di Cintio et al. 2014b profile – produces similar results when applied to both simulated and real data; Allaert, Gentile & Baes 2017; Schneider et al. 2017.)

In Fig. 1, we show fits to the DM density profiles of haloes extracted from pure DM cosmological simulations in ΛCDM, with virial masses over range: $10^9 < M_{200}/{\rm M}_\odot < 10^{11}$, corresponding to dwarf galaxies. The median lines assume that haloes lie on the M_{200}–c_{200} relation (equation 5), while the shaded regions show the 1σ scatter in this relation. The purple line shows a maximally cored DM halo (equation 9) with $M_{200} = 10^{10}\,{\rm M}_\odot$, $n = 1$, and $R_{1/2} = 0.015\,r_{200} = 0.7$ kpc (Kravtsov 2013), corresponding to $r_{\rm c} = 1.2$ kpc. This cored model gives a good match to simulations in which DM cusps are transformed to cores by gas flows (Read et al. 2016a), but also to models in which cores form due to self-interactions between DM particles (Schneider et al. 2017; Read et al. 2018). The key difference between these two models, as highlighted in Introduction, is that the former predicts an anticorrelation

between the DM core size and the total amount of star formation in a dwarf galaxy (i.e. the longer the star formation continues, the more times gas cycles in and out of the centre of the dwarf and the more DM heating occurs), while the latter predicts no such anticorrelation. This is the key difference that we set out to test in this paper.

The striking thing to note from Fig. 1 is just how different the central densities of the cored and cusped models are, independently of halo mass M_{200}. While a measurement of the *slope* of the density profile is ideal for differentiating models, we can actually differentiate among these cored and cusped models with a single measurement of the density at small radii. In this paper, we choose this 'small radius' to be $r_S = 150$ pc (vertical grey line). This represents a compromise between picking r_S small enough to differentiate between interesting models, but not so small that the uncertainties on $\rho_{\rm DM}(r_S)$ are prohibitively large. In Appendix C, we show that our results are not sensitive to this choice of r_S.

The inner logarithmic slope of the density profile, $\gamma_{\rm DM}(r_S) \equiv {\rm d}\ln\rho_{\rm DM}/{\rm d}\ln r(r_S)$, or the asymptotic slope, $\gamma_{\rm DM}(r \to 0)$, have traditionally be used to differentiate cored and cusped models (e.g. Hague & Wilkinson 2013). However, as can be seen in Fig. 1, we can obtain useful cosmological information also from the amplitude of the DM density profile at $r_S = 150$ pc. In Read et al. (2018), we used mock data for a Draco-like dwarf to show that, with ∼500 stars with radial velocities, GravSphere's inference of $\gamma_{\rm DM}(150\,{\rm pc})$ depended on our choice of priors on $\gamma_{\rm DM}$. By contrast, GravSphere's inference of $\rho_{\rm DM}(150\,{\rm pc})$ was not sensitive to these priors. For this reason, we focus in this paper primarily on $\rho_{\rm DM}(150\,{\rm pc})$. For completeness, we show results for $\gamma_{\rm DM}(150\,{\rm pc})$ in Appendix D.

3 METHOD

3.1 Modelling the stellar kinematics: GravSphere

GravSphere is described and tested in detail in Read & Steger (2017) and Read et al. (2018). It solves the projected spherical Jeans equation (Jeans 1922; Binney & Mamon 1982):

$$\sigma^2_{\rm LOS}(R) = \frac{2}{\Sigma(R)}\int_R^\infty \left(1-\beta\frac{R^2}{r^2}\right)\nu\sigma_r^2\,\frac{r\,{\rm d}r}{\sqrt{r^2-R^2}} \tag{10}$$

where $\Sigma(R)$ denotes the tracer surface mass density at projected radius R; $\nu(r)$ is the spherically averaged tracer density; and $\beta(r)$ is the velocity anisotropy:

$$\beta = 1 - \frac{\sigma_{\rm t}^2}{\sigma_{\rm r}^2} \tag{11}$$

where $\sigma_{\rm t}$ and $\sigma_{\rm r}$ are the tangential and radial velocity dispersions, respectively, and $\sigma_{\rm r}$ is given by (van der Marel 1994; Mamon & Łokas 2005):

$$\sigma_r^2(r) = \frac{1}{\nu(r)g(r)}\int_r^\infty \frac{GM(\tilde{r})\nu(\tilde{r})}{\tilde{r}^2}g(\tilde{r}){\rm d}\tilde{r} \tag{12}$$

where:

$$g(r) = \exp\left(2\int\frac{\beta(r)}{r}{\rm d}r\right) \tag{13}$$

and $M(r)$ is the cumulative mass of the dwarf galaxy (due to all stars, gas, DM etc.), that we would like to measure.

GravSphere uses a non-parametric model for $M(r)$ that comprises a contribution from all visible matter and a contribution from DM that is described by a sequence of power laws defined on a set of radial bins. In this paper, these bins are defined at [0.25, 0.5, 1, 2, 4]$R_{1/2}$, where $R_{1/2}$ is the projected half-light radius of the tracer stars. The tracer light profile is also non-parametric, using a series sum of Plummer spheres, as in Rojas-Niño et al. (2016). The velocity anisotropy is given by a form that makes $g(r)$ analytic:

$$\beta(r) = \beta_0 + (\beta_\infty - \beta_0)\frac{1}{1+\left(\frac{r_0}{r}\right)^n} \tag{14}$$

where β_0 is the inner asymptotic anisotropy, β_∞ is the outer asymptotic anisotropy, r_0 is a transition radius, and n controls the sharpness of the transition.

We use a symmetrized $\tilde{\beta}$ (Read et al. 2006b; Read & Steger 2017):

$$\tilde{\beta} = \frac{\sigma_{\rm r}^2 - \sigma_{\rm t}^2}{\sigma_{\rm r}^2 + \sigma_{\rm t}^2} = \frac{\beta}{2-\beta} \tag{15}$$

since this avoids infinities in β for highly tangential orbits. We assume flat priors on $-1 < \tilde{\beta}_{0,\infty} < 1$ such that we give equal weight to tangentially and radially anisotropic models.

By default, GravSphere also fits for the two higher order 'VSPs' (Merrifield & Kent 1990; Richardson & Fairbairn 2014; Read & Steger 2017):

$$v_{\rm s1} = \frac{2}{5}\int_0^\infty GM\,(5-2\beta)\,\nu\sigma_{\rm r}^2\,r\,{\rm d}r \tag{16}$$

$$= \int_0^\infty \Sigma\langle v_{\rm LOS}^4\rangle\,R\,{\rm d}R \tag{17}$$

and:

$$v_{\rm s2} = \frac{4}{35}\int_0^\infty GM\,(7-6\beta)\,\nu\sigma_{\rm r}^2\,r^3\,{\rm d}r \tag{18}$$

$$= \int_0^\infty \Sigma\langle v_{\rm LOS}^4\rangle\,R^3\,{\rm d}R\,. \tag{19}$$

These allow GravSphere to break the $\rho-\beta$ degeneracy (Read & Steger 2017). We use the improved estimators for $v_{\rm s1}$ and $v_{\rm s2}$ described in Read et al. (2018).

GravSphere fits the above model to the surface density profile of tracer stars, $\Sigma_*(R)$, their line-of-sight projected velocity dispersion profile $\sigma_{\rm LOS}(R)$ and their VSPs using the EMCEE affine invariant Markov Chain Monte Carlo sampler from Foreman-Mackey et al. (2013). We assume uncorrelated Gaussian errors such that the Likelihood function is given by $\mathcal{L} = \exp(-\chi^2/2)$, where χ^2 includes the contributions from the fits to Σ_*, $\sigma_{\rm LOS}$, and the two VSPs. We use 1000 walkers, each generating 5000 models and we throw out the first half of these as a conservative 'burn in' criteria. [See Read & Steger (2017) and Read et al. (2018) for further details of our methodology and priors.]

GravSphere has been extensively tested on mock data with realistic contamination and selection criteria, realistic departures from spherical symmetry and realistic disequilibrium due to tidal stripping (Read & Steger 2017; Read et al. 2018). In all cases, GravSphere was able to recover the key quantity of interest for this paper – $\rho_{\rm DM}(150\,{\rm pc})$ – within its 95 per cent confidence intervals.

3.2 Fitting gaseous rotation curves

For the gas-rich isolated dwarfs, we derive the rotation curves from HI datacubes using the 3DBarolo software, as in Read et al. (2017) and Iorio et al. (2017). For the mass model, we decompose the circular speed curve into contributions from stars, gas, and DM:

$$v_{\rm c}^2 = v_*^2 + v_{\rm gas}^2 + v_{\rm dm}^2 \tag{20}$$

where v_* and $v_{\rm gas}$ are the contributions from stars and gas, respectively, and $v_{\rm dm}$ is the DM contribution.

We assume that both the stars and gas are exponential discs:

$$v^2_{*/\rm gas} = \frac{2GM_{*/\rm gas}}{R_{*/\rm gas}} y^2 \left[I_0(y)K_0(y) - I_1(y)K_1(y)\right] \quad (21)$$

where $M_{*/\rm gas}$ is the mass of the star/gas disc, respectively; $R_{*/\rm gas}$ is the exponential scale length; $y = R/R_{*/\rm gas}$ is a dimensionless radius parameter; and I_0, I_1, K_0, and K_1 are Bessel functions (Binney & Tremaine 2008). As in Read et al. (2017), we fix the values of R_*, $R_{\rm gas}$, and $M_{\rm gas}$ to the median of their observed values in our model fits. All values used are reported in Table 1.

To ensure consistency between the stellar kinematic and gas-rich models that we presented here, for the DM mass distribution ($v^2_{\rm dm} = GM_{\rm dm}/r$), we use the freeform mass model from Read & Steger (2017), described in Section 3.1, above. This differs from the analysis in Read et al. (2016b, 2017) where we used instead the 'coreNFW' profile from Read et al. (2016a). In tests, we verified that this choice does not affect our results. (Using the coreNFW distribution instead, and allowing the core-size parameter, $r_{\rm c}$, to freely vary, leads to density profiles consistent with our freeform models, but with smaller uncertainties corresponding to the reduced freedom in the mass model.)

4 THE DATA

Our data sample comprises nearby dwarf galaxies that – based on mock data tests – have sufficiently good data to estimate $\rho_{\rm DM}(150\,{\rm pc})$ reliably, and that have had their data analysed in a homogeneous manner. These are the eight Milky Way 'classical' dSphs (e.g. McConnachie 2012), and eight isolated gas-rich dIrr galaxies taken from Read et al. (2017).

4.1 The dwarf irregulars

For the isolated dIrrs, we measure their DM density profile from their HI gas rotation curves, as described in Read et al. (2017) and Section 3.2. The rotation curves for these galaxies were extracted from the HI datacubes using $^{\rm 3D}$BAROLO, as described in detail in Read et al. (2017) and Iorio et al. (2017). As in Read et al. (2017), our isolated dwarf sample is chosen to have an inclination angle of $i > 40^\circ$ because $^{\rm 3D}$BAROLO can become systematically biased for lower inclination angles than this. We also require a good measurement of the distance and photometric light profile (Read et al. 2016b). Two of the dwarfs, WLM and Aquarius, have SFHs derived from deep colour–magnitude diagrams (Dolphin 2000; Cole et al. 2014); the remainder are known to be still forming stars today (Zhang et al. 2012). Finally, of the 11 dwarfs in Read et al. (2017) that meet the above criteria, we exclude NGC 6822 because it has a central stellar bar that complicates the analysis, and DDO 126 and UGC 8505 because their inner rotation curves are sufficiently uncertain that we are unable to obtain a good measurement of $\rho_{\rm DM}(150\,{\rm pc})$. The data for our sample of dIrrs are described and presented in detail in Read et al. (2017) and Iorio et al. (2017) and so we refer the reader to those publications for further details.

4.2 The dwarf spheroidals

Our sample of dSphs: Draco, UMi, Sculptor, Carina, Fornax, Sextans, Leo I, and Leo II, each have $\gtrsim 190$ stars with radial velocities and well-measured photometric light profiles. The best-sampled systems have over 500 member velocities (Draco [504], Carina [767], Sculptor [1351], and Fornax [2573]). We mass model these dSphs using the GravSphere code (see Read & Steger 2017; Read et al. 2018 and Section 3.1). With $\sim$500 member velocities, GravSphere can estimate $\rho_{\rm DM}(150\,{\rm pc})$ well enough to distinguish a ΛCDM cusp from a constant density core at 95 per cent confidence (see Sections 2 and 3.1). GravSphere gracefully degrades as the number of data points are reduced.

Since GravSphere simultaneously fits both surface density and projected velocity dispersion profiles, for each dSph, we require both photometric and kinematic data. For the photometric data, we use the Panoramic Survey Telescope and Rapid Response System (Pan-STARRS) DR1 catalogue (Flewelling et al. 2016) for the northern dwarfs Draco, Leo I, Leo II, Sextans, and Ursa Minor. For the southern dwarfs Fornax and Scuptor, we use data from the VLT/ATLAS DR1 catalogue, as re-processed and calibrated by Koposov et al. (2014). For the southern dwarf Carina, which is not included in either of the above catalogues, we use a catalogue derived from observations with the Dark Energy Camera by McMonigal et al. (2014) and generously provided by those authors (McMonigal, private communication). From each photometric catalogue we initially select point-like sources[6] within circular apertures of sufficient angular radius (1.5° for each of Draco, Fornax, Sculptor, Sextans, and Ursa Minor; 1° for Leo I and Leo II and 0.9° for Carina) to enclose all plausibly bound member stars. From these point sources we obtained samples of candidate red giant branch (RGB) stars within each dwarf galaxy by selecting only sources that are brighter than $i \leq 21$ mag and that deviate in colour–magnitude ($g - r$, i) space by less than ε magnitudes from an old (age=12 Gyr), metal-poor ([Fe/H] $= -2.5$) model isochrone (Dotter et al. 2008) that we shift by the distance modulus corresponding to each galaxy's published distance (McConnachie 2012). The only exception is Carina, for which i-band data are not available and we use g instead, keeping the same magnitude limit of $g \leq 22$. For this work, we adopt $\epsilon = \sqrt{0.04 + \sigma_{\rm i}^2 + \sigma_{\rm g-r}^2}$, where $\sigma_{\rm i}$ and $\sigma_{\rm g-r}$ are the photometric uncertainties in magnitude and colour, respectively.

For the stellar-kinematic data, we use the published spectroscopic samples of Walker, Mateo & Olszewski (2009) for Carina, Fornax, Sculptor and Sextans, Mateo, Olszewski & Walker (2008) for Leo I, Spencer et al. (2017) for Leo II, and Walker, Olszewski & Mateo (2015) for Draco. For Ursa Minor, we use spectroscopic data that were acquired, processed, and analysed in the same way as that of Draco (Spencer et al. 2018). In addition to line-of-sight velocities, these data sets contain information about the chemical composition of individual stars, in the form either of a magnesium index (Walker et al. 2009) or a direct estimate of [Fe/H] (Walker et al. 2015); the only exception is Leo I, for which only velocities are available. In order to separate dwarf galaxy members from contamination from the Galactic foreground, we fit an initial, chemodynamical mixture model that is similar to the one described in detail by Caldwell et al. (2017); the only difference is that here we assume any velocity and/or metallicity gradients are negligible. After fitting these simple models, we evaluate for every individual

[6]For the Pan-STARRS catalogues, we select point sources as objects for which the difference between point spread function (PSF) and Kron magnitudes in the r band is $r_{\rm PSF} - r_{\rm kron} < 0.05$ (see Farrow et al. 2014 for a discussion of Pan-STARRS star–galaxy separation). For the ATLAS catalogues, we select objects classified as stars (star/galaxy classifier value of -1). For Carina, we use objects classified as stars by McMonigal et al. (2014).

Table 1. Data for the eight dSph and eight dIrr galaxies we study in this work. From left to right, the columns give: the name of the galaxy; type (dSph or dIrr); distance from the centre of the Milky Way; stellar mass; gas mass (for the dIrrs); stellar half-light radius, $R_{1/2}$; exponential gas scale length (for the dIrrs); the pre-infall halo mass estimated from HI rotation curves (for the dIrrs) or abundance matching (for the dSphs; see Section 5.4); the number of kinematic member stars (for the dSphs); the star formation truncation time (defined in Introduction); and our estimates of $\rho_{\rm DM}(150\,{\rm pc})$ and $\gamma_{\rm DM}(150\,{\rm pc})$ with their 68 per cent confidence intervals (see Section 5.4). For the dSphs, the column giving $R_{1/2}$ quotes literature values compiled in the McConnachie (2012) review and, in square brackets, the value favoured for our sample of RGB stars by GravSphere. This is in excellent agreement with the literature values for all dSphs except Sextans and UMi, where GravSphere favours a smaller and larger $R_{1/2}$, respectively. Finally, the last column gives the data references for each galaxy, as follows: 1: Read et al. (2017); 2: Dolphin (2000); 3: McConnachie (2012); 4: Aparicio et al. (2001); 5: Carrera et al. (2002); 6: de Boer et al. (2012a); 7: Lee et al. (2009); 8: Dolphin (2002); 9: de Boer et al. (2014); 10: de Boer et al. (2012b). The references for the photometric and kinematic data for the dSphs are given in Section 4.

Galaxy	Type	D (kpc)	M_* ($10^6\,{\rm M}_\odot$)	$M_{\rm gas}$ ($10^6\,{\rm M}_\odot$)	$R_{1/2}$ (kpc)	$R_{\rm gas}$ (kpc)	M_{200} ($10^9{\rm M}_\odot$)	Sample size	$t_{\rm trunc}$ (Gyr)	$\rho_{\rm DM}(150\,{\rm pc})$ ($10^8{\rm M}_\odot\,{\rm kpc}^{-3}$)	$\gamma_{\rm DM}(150\,{\rm pc})$	Refs.
UMi	dSph	76 ± 3	0.29	–	0.181 ± 0.027 [0.306]	–	2.8 ± 1.1	430	12.4	$1.53^{+0.35}_{-0.32}$	$-0.71^{+0.28}_{-0.29}$	3,5
Draco	dSph	76 ± 6	0.29	–	0.221 ± 0.019 [0.198]	–	1.8 ± 0.7	504	11.7	$2.36^{+0.29}_{-0.29}$	$-0.95^{+0.25}_{-0.25}$	3,4
Sculptor	dSph	86 ± 6	2.3	–	0.283 ± 0.045 [0.248]	–	5.7 ± 2.3	1351	11.8	$1.49^{+0.28}_{-0.23}$	$-0.83^{+0.3}_{-0.25}$	3,6
Sextans	dSph	86 ± 4	0.44	–	0.695 ± 0.044 [0.352]	–	2.0 ± 0.8	417	10.6	$1.28^{+0.34}_{-0.29}$	$-0.95^{+0.36}_{-0.41}$	3,7
Leo I	dSph	254 ± 15	5.5	–	0.251 ± 0.027 [0.298]	–	5.6 ± 2.2	328	3.1	$1.77^{+0.33}_{-0.34}$	$-1.15^{+0.33}_{-0.37}$	3,8
Leo II	dSph	233 ± 14	0.74	–	0.176 ± 0.042 [0.194]	–	1.6 ± 0.7	186	6.3	$1.84^{+0.17}_{-0.16}$	$-1.5^{+0.35}_{-0.31}$	3,8
Carina	dSph	105 ± 6	0.38	–	0.250 ± 0.039 [0.242]	–	0.8 ± 0.30	767	2.8	$1.16^{+0.20}_{-0.22}$	$-1.23^{+0.39}_{-0.35}$	3,9
Fornax	dSph	138 ± 8	43	–	0.710 ± 0.077 [0.670]	–	21.9 ± 7.4	2573	1.75	$0.79^{+0.27}_{-0.19}$	$-0.30^{+0.21}_{-0.28}$	3,10
WLM	dIrr	985 ± 33	16.2 ± 4	79	1.26	1.04	8.3^{+2}_{-2}	–	0	$0.52^{+0.09}_{-0.09}$	$-0.37^{+0.19}_{-0.16}$	1,2
DDO 52	dIrr	10,300	52.7 ± 13	371	1.58	2.49	$12^{+2.9}_{-2.7}$	–	0	$0.38^{+0.17}_{-0.10}$	$-0.18^{+0.13}_{-0.24}$	1
DDO 87	dIrr	7,400	33 ± 8	310	1.9	1.51	$11.3^{+2.7}_{-2.5}$	–	0	$0.31^{+0.18}_{-0.09}$	$-0.22^{+0.15}_{-0.24}$	1
DDO 154	dIrr	3,700	8.35 ± 2	309	0.91	2.34	$12.6^{+0.5}_{-0.5}$	–	0	$0.46^{+0.13}_{-0.10}$	$-0.20^{+0.15}_{-0.24}$	1
Aquarius	dIrr	900	0.68 ± 0.17	3.3	0.37	0.25	$0.68^{+1.3}_{-0.4}$	–	0	$0.36^{+0.22}_{-0.19}$	$-0.41^{+0.31}_{-0.51}$	1
NGC 2366	dIrr	3,400	69.5 ± 17.3	1,730	1.54	2.69	$24^{+4.9}_{-5.4}$	–	0	$0.18^{+0.05}_{-0.03}$	$-0.09^{+0.07}_{-0.12}$	1
CVnIdwA	dIrr	3,600	4.1 ± 1	64.2	1.14	1.18	$1.7^{+1}_{-0.5}$	–	0	$0.33^{+0.12}_{-0.09}$	$-0.25^{+0.17}_{0.27}$	1
DDO 168	dIrr	4,300	59 ± 14.8	458	1.38	1.51	$21^{+5.2}_{-4.8}$	–	0	$0.31^{+0.11}_{-0.07}$	$-0.14^{+0.11}_{-0.18}$	1

star a probability of dwarf galaxy membership, $P_{\rm mem}$, according to equation (7) of Caldwell et al. (2017, for RGB candidates lacking spectroscopic measurements, we evaluate membership probability based only on projected distance from the dwarf galaxy centre). We then construct empirical surface density and projected velocity dispersion profiles by dividing the photometric and spectroscopic data sets, respectively, into annular bins that each contain equal numbers (weighted by membership probability) of member stars. We confirm that our results are qualitatively unchanged for alternative profiles that use different numbers of bins and/or membership probabilities obtained from more sophisticated initial models (e.g. ones that explicitly allow for radially varying velocity dispersion).

4.3 Star formation histories

For the SFHs, where possible we use literature determinations derived from deep resolved colour–magnitude diagrams (Draco, Aparicio, Carrera & Martínez-Delgado 2001; Sculptor, de Boer et al. 2012a; Carina, de Boer et al. 2014; Sextans, Lee et al. 2009; UMi, Carrera et al. 2002; Leo I, Dolphin 2002, Leo II, Dolphin 2002, WLM, Dolphin 2000; Aquarius, Cole et al. 2014). For the remainder of our sample of dIrrs – that are all still star forming today – we use the SFH measured from their integrated light by Zhang et al. (2012).

4.4 Dark matter halo masses

We obtain M_{200} for our sample of dIrrs by using an extrapolation from their HI rotation curves (Read et al. 2017). For our sample of dSphs, we use estimates from a novel form of abundance matching that corrects for satellite quenching on infall (Read & Erkal 2018). As discussed in Read et al. (2017) and Read & Erkal (2018), these abundance matching estimates of M_{200} agree remarkably well with dynamical estimates from HI rotation curves or stellar kinematics. In Section 5, we show that our results are not sensitive to even rather large systematic errors in our estimates of M_{200}.

Our full data sample, including half-light radii, stellar masses, HI masses, stellar kinematic sample size, and data references are given in Table 1. There, we also report $t_{\rm trunc}$ for each dwarf (see Introduction), M_{200} (see above), and our estimates of $\rho_{\rm DM}(150\,{\rm pc})$ (see Section 5), and $\gamma_{\rm DM}(150\,{\rm pc})$ (see Appendix D).

5 RESULTS

5.1 Example GravSphere model fits and constraints on the velocity anisotropy profile

Before addressing the primary goal of this work – the DM density profiles – in Fig. 2, we show three example GravSphere model fits for Draco (top), Sculptor (middle), and Fornax (bottom). (The other dSph fits are similar to these and so we omit them for brevity.) The panels show, from left to right, the projected velocity dispersion $\sigma_{\rm LOS}$, the tracer surface density profile, Σ_*, and the symmetrized velocity anisotropy profile, $\tilde{\beta}$ (see equation 15). The data with errors are shown by the blue points, the contours mark the 68 per cent (dark grey) and 95 per cent (light grey) confidence intervals of our GravSphere models, and the vertical blue lines mark the projected half-light radius, $R_{1/2}$.

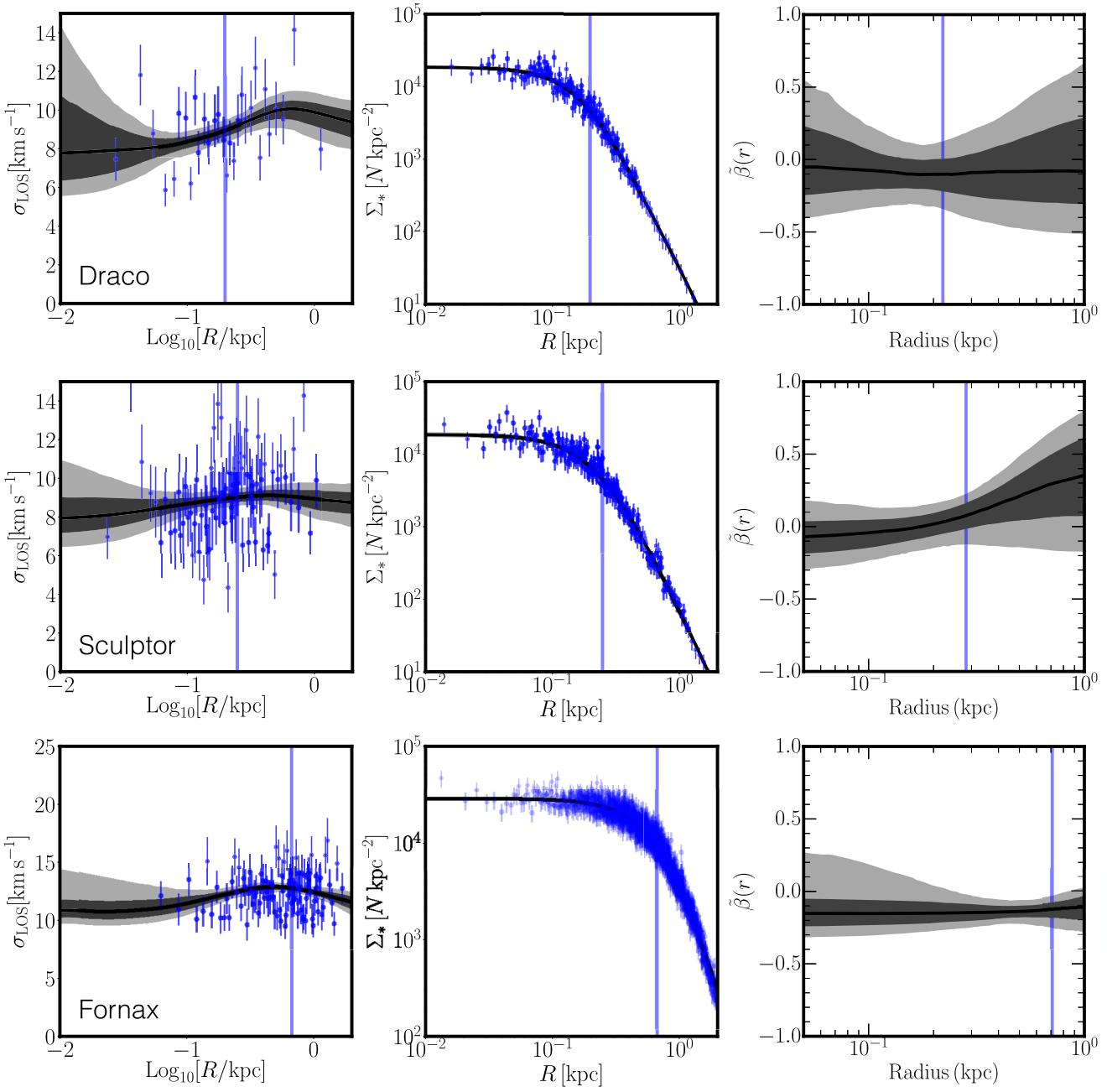

Figure 2. Example GRAVSPHERE model fits for Draco (top), Sculptor (middle), and Fornax (bottom). The panels show, from left to right, the projected velocity dispersion $\sigma_{\rm LOS}$, the tracer surface density profile, Σ_*, and the symmetrized velocity anisotropy profile, $\tilde{\beta}$ (see equation 15). The data with errors are shown by the blue points, the contours mark the 68 per cent (dark grey), and 95 per cent (light grey) confidence intervals of our GRAVSPHERE models, and the vertical blue lines mark the projected half-light radius, $R_{1/2}$. From top to bottom, these three dSphs demonstrate the effect of increasing the number of member velocities, from 504 in Draco to 1351 in Sculptor and 2573 in Fornax. Notice how the constraints on $\tilde{\beta}$ improve with improved spectroscopic sampling.

The three dSphs in Fig. 2 have an increasing number of member velocities, from 504 in Draco to 1351 in Sculptor and 2573 in Fornax. This demonstrates how the GRAVSPHERE model fits improve with increasing sampling. Notice that in all cases, the GRAVSPHERE models provide good fits to the binned data. Both VSPs (see Section 3.1) are also well fitted for all three dwarfs, with no indication of bias due to triaxiality (see Read & Steger 2017 for a discussion of this). The Draco model fits are discussed in detail in a separate companion paper where we use Draco – that is the densest of our full dwarf sample – to place constraints on SIDM models (Read et al. 2018).

For all of the dSphs that we study in this work, our GRAVSPHERE models are consistent with being isotropic within their 95 per cent confidence intervals. The majority have strong constraints only near $R_{1/2}$ (cf. the results for Draco in the top right panel of Fig. 2). However, for Sculptor and Fornax, that have the largest number of member velocities, we are able to constrain $\tilde{\beta}$ also at larger and smaller radii. For Sculptor, we weakly favour isotropic models

near the centre that become radially anisotropic for $R > R_{1/2}$ (see Fig. 2, middle row, right-hand panel). For Fornax, we weakly favour some tangential anisotropy at all radii (see Fig. 2, bottom row, right-hand panel). Tangential anisotropy has been noted in some previous studies of Fornax (e.g. Breddels et al. 2013; Kowalczyk et al. 2018). However, for our GravSphere models, the evidence for this anisotropy is marginal.

5.2 Dark matter density profiles

In Fig. 3, we show our results for the radial DM density profiles of dSphs with >500 member velocities, and two dIrrs – WLM and Aquarius – that have a well-measured SFH (see Section 4). The left-hand panel shows the SFH, where an age of zero corresponds to today, while the beginning of the Universe is on the right of the plot at ∼14 Gyr. All plots are normalized such that the integral of the SFR over $t_{\rm univ} = 13.8$ Gyr matches the stellar masses reported in Table 1. The middle and right-hand panels show the radial DM density profiles. The light and dark contours mark the 95 per cent and 68 per cent confidence intervals of our models, respectively. The vertical grey lines mark the projected half-light radius, $R_{1/2}$. For the dSphs, the DM density profile is derived from the stellar kinematics (Section 3.1), while for the dIrrs, it is derived from the HI gas rotation curve (Section 3.2). For Aquarius, there are also stellar radial velocities available for ∼25 member stars[7] (Kirby et al. 2014). The purple dashed lines mark the 68 per cent confidence intervals of GravSphere models applied to these data. This demonstrates the consistency between our stellar kinematic and HI gas mass modelling, but – as anticipated from tests on mock data in Read & Steger (2017) – with just 25 member velocities, GravSphere is not able to well constrain the DM density inside $R < R_{1/2}$ for Aquarius.

First, notice that the GravSphere models for Draco favour a high central density inside $R < R_{1/2}$, consistent with a ΛCDM cusp. Below the contours of the GravSphere models, we mark on two power-law density profiles, $\rho \propto r^{-1}$ (cusp) and $\rho = $ const. (core). [We discuss Draco, the densest dwarf of our full sample, in detail in a companion paper (Read et al. 2018).] The GravSphere models for Sculptor, that formed ∼8 times more stars than Draco, favour a lower central density than Draco, consistent with both an inner core and a cusp within GravSphere's 95 per cent confidence intervals. This trend of decreasing inner density with increasing star formation is seen also in Fornax. The GravSphere models for Fornax – that formed nearly 150 times more stars than Draco – is less dense than both Draco and Sculptor, with $\rho_{\rm DM}(150\,{\rm pc})$ a factor of ∼3 lower than for Draco. This shallow inner density profile for Fornax is remarkably similar to that for WLM (compare the middle and right-hand panels in the middle row of Fig. 3). This is interesting since WLM and Fornax share similar SFHs (see Fig. 3, middle row, left-hand panel) up until ∼2 Gyr ago when Fornax's star formation quenched. Our GravSphere models for Aquarius, despite having substantially larger uncertainties than WLM, also favour a low inner DM density within their 95 per cent confidence intervals. Finally, Carina is an interesting case. It has formed stars for nearly a full Hubble time, but despite its substantially more extended star formation, it formed only ∼30 per cent more stars than Draco. Our GravSphere models for Carina weakly favour a dense 'cuspy' profile, similar to that for Draco, but also permit a low-density core within their 95 per cent confidence intervals (see Fig. 3, bottom row). We discuss Carina further in Section 6.

In Fig. 4, we show the results for our sample of dSphs with <500 member velocities. For these galaxies, we expect the GravSphere model constraints to be poorer and in general the confidence intervals of our models are broader for these dSphs. None the less, we remain able to detect that Leo I and Leo II are substantially more dense than Fornax, while Sextans and UMi favour a density similar to Sculptor and Carina that lies in-between that of Draco and Fornax. Finally, in Appendix A (Fig. A1), we show the results for the remainder of our sample of dIrrs. These all have similar DM density profiles that are consistent with constant density cores, as has been reported previously in the literature (e.g. Oh et al. 2015; Read et al. 2017).

5.3 A diversity of central dark matter densities

In Figs 3 and 4, we saw that our sample of dwarfs have a wide range of DM density profiles. In particular, their central densities appeared to decrease with increasing star formation. In this section, we study this diversity quantitatively. In Fig. 5, left-hand panel, we plot $\rho_{\rm DM}(150\,{\rm pc})$ for our full sample of dwarfs (see Section 2) as a function of their stellar masses, M_*. The data points are coloured by their star formation truncation times, $t_{\rm trunc}$, as marked in the legend (see Section 4 and Table 1). Notice that the dwarfs fall into two broad classes. Those with only old stars ($t_{\rm trunc} > 6$ Gyr; black) have $\rho_{\rm DM}(150\,{\rm pc}) > 10^8\,{\rm M}_\odot\,{\rm kpc}^{-3}$, while those with extended star formation ($t_{\rm trunc} < 3$ Gyr; blue) have $\rho_{\rm DM}(150\,{\rm pc}) < 10^8\,{\rm M}_\odot\,{\rm kpc}^{-3}$. Note, however, that Carina, UMi, and Sextans are possible exceptions to this. They could lie on either side of this boundary within their 95 per cent confidence intervals. This could imply a continuum of central DM densities rather than a dichotomy. However, the uncertainties on $\rho_{\rm DM}(150\,{\rm pc})$ are currently too large to determine whether or not this is the case. We discuss this further in Section 6.

Finally, notice that there are several dwarfs – UMi, Draco, Carina, Sextans, Leo II, and Aquarius – with similar baryonic mass but very different $\rho_{\rm DM}(150\,{\rm pc})$. In Appendix B, we show that this is challenging to understand in 'alternative gravity' theories for DM.

5.4 Evidence for dark matter heating in dwarf galaxies

From Fig. 5 (left-hand panel), we see a significant scatter in the central DM densities of nearby dwarf galaxies at a similar stellar mass. In this section, we consider three physical effects that could induce this scatter in ΛCDM. First, ram pressure from the Milky Way's hot corona will cause star formation in the dwarfs to rapidly shut down on infall (e.g. Gatto et al. 2013). This will induce scatter in M_* at a fixed pre-infall halo mass, M_{200}, leading to a range of M_* at a given $\rho_{\rm DM}(150\,{\rm pc})$ (e.g. Read et al. 2017). Secondly, tidal shocking and stripping can lower the central DM density of the dwarfs, inducing scatter in $\rho_{\rm DM}(150\,{\rm pc})$ at a fixed M_* (e.g. Hayashi et al. 2003; Kazantzidis et al. 2004; Read et al. 2006a). And thirdly, 'DM heating' will push DM out of the centres of the dwarfs. At fixed M_{200}, this leads to a lower $\rho_{\rm DM}(150\,{\rm pc})$ for a larger M_* (see Introduction).

First, note that while tidal stripping is likely to affect the outer DM profiles of the dSphs, for the orbits that the classical dwarfs are known to move on, the effect of tidal stripping and shocking on the profile inside $R_{1/2}$ is expected to be small (e.g. Hayashi et al. 2003;

[7]Note that stellar kinematic data are also available for WLM (Leaman et al. 2012). However, there is evidence for rotation in these stars which cannot currently be included in the GravSphere models. We will revisit joint constraints from combined stellar and gas kinematics in future work.

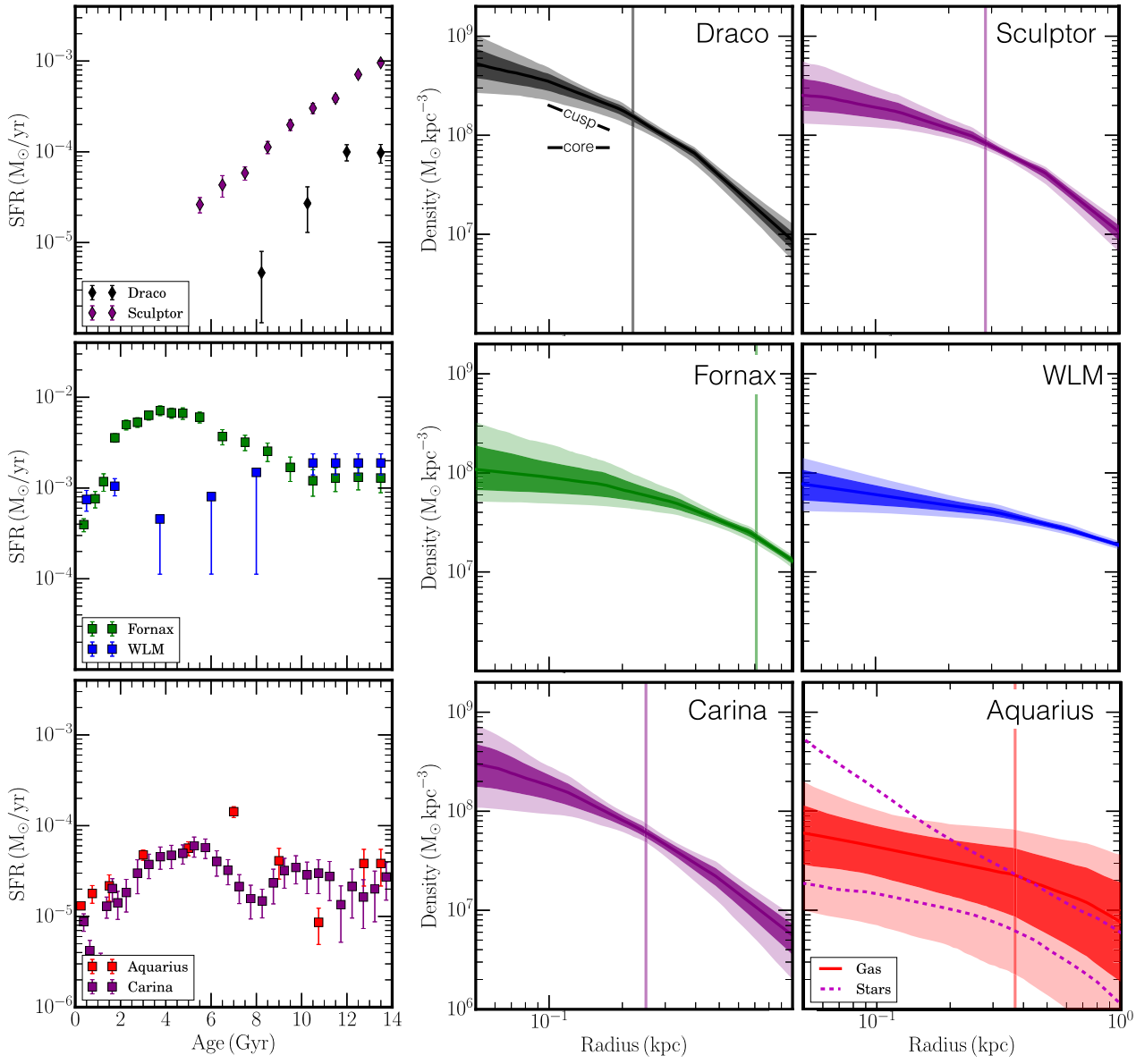

Figure 3. The radial DM density profiles of dSphs with >500 member velocities, and two dIrrs (WLM and Aquarius) with a well-measured SFH (see Section 4). The left-hand panel shows the SFH, where today is on the left, while the beginning of the Universe is on the right of the plot. All plots are normalized such that the integral of the SFR over $t_{\rm univ} = 13.8$ Gyr matches the stellar masses reported in Table 1. The middle and right-hand panels show the radial DM density profiles. The light and dark contours mark the 95 per cent and 68 per cent confidence intervals of our models, respectively. The vertical grey lines mark the projected half-light radius, $R_{1/2}$. For the dSphs, the DM density profile is derived from the stellar kinematics (Section 3.1), while for the dIrrs, it is derived from the HI gaseous rotation curve (Section 3.2). For Aquarius, there are also stellar radial velocities available for ∼25 member stars. The purple dashed lines mark the 68 per cent confidence intervals of GravSphere models applied to these data.

Kazantzidis et al. 2004; Read et al. 2006a,b; Peñarrubia, Navarro & McConnachie 2008; Lux, Read & Lake 2010; Gaia Collaboration et al. 2018; Read et al. 2018). Furthermore, tides cannot affect the isolated dIrrs, yet these have a *lower* $\rho_{\rm DM}(150\,{\rm pc})$ than most of the dSphs (Fig. 5, left-hand panel). Of the mechanisms we consider here, this leaves ram pressure stripping and DM heating as the main sources of scatter.

Ram-pressure-induced scatter in $\rho_{\rm DM}(150\,{\rm pc})$ at a fixed M_* is caused, ultimately, by the dwarfs inhabiting haloes with very different pre-infall masses, M_{200}. Thus, if we can obtain an independent estimate of M_{200} for our dwarf sample, then we can remove this source of scatter. As discussed in Section 4, for the isolated dIrrs we obtain an extrapolated M_{200} directly from their HI rotation curves (Read et al. 2017), while for the dSphs, we obtain M_{200} by abundance matching with their mean SFRs (Read & Erkal 2018). We report these M_{200} for our full sample, with uncertainties, in Table 1.

In Fig. 5 (middle panel), we plot $\rho_{\rm DM}(150\,{\rm pc})$ as a function of M_{200} for our full dwarf sample. The grey band marks the expected range of inner DM densities of ΛCDM haloes assuming no cusp–core transformations take place (i.e. assuming NFW profiles), where the width of the band accounts for the 1σ scatter in the $M_{200}-c_{200}$ relation (see equations 1 and 5 and Fig. 1). The blue band marks the same, but for the coreNFW profile, assuming maximal core

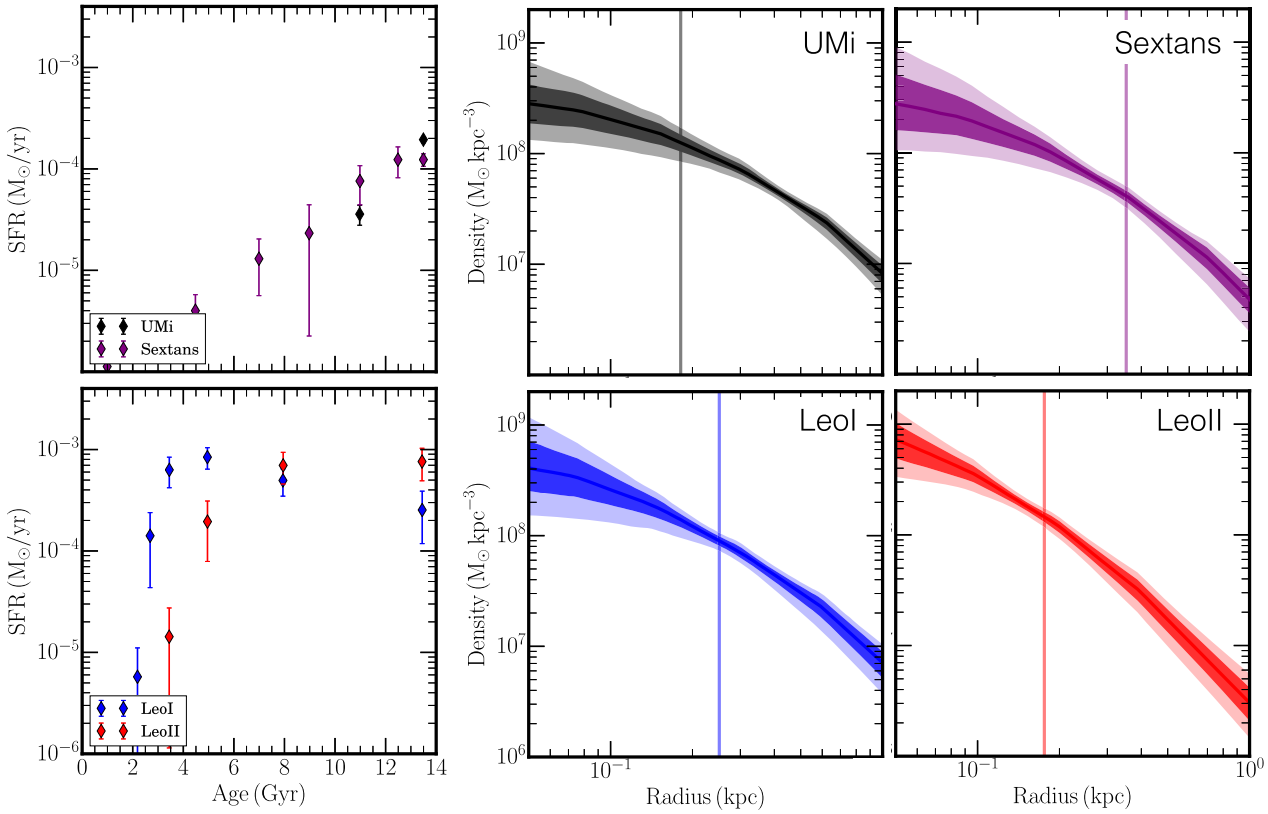

Figure 4. As Fig. 3, but for dSphs with <500 member velocities.

formation (equation 6). Thus, the grey and blue bands bracket the extremum cases of no cusp–core transformation and complete cusp–core transformation in ΛCDM.

From Fig. 5 (middle panel), we can see that the dwarfs with extended star formation (blue) have low central DM densities and lie along the blue track, consistent with DM cores, while those whose star formation shut down long ago (black) lie along the grey track, consistent with DM cusps. The uncertainties on $\rho_{\rm DM}(150\,{\rm pc})$ and M_{200} are currently too large to be able to definitively place any of the dwarfs in the 'transition' region between being fully cusped (grey) and fully cored (blue). We discuss this further in Section 6.

To further illustrate the above result, in Fig. 5 (right-hand panel), we plot $\rho_{\rm DM}(150\,{\rm pc})$ for our sample of dwarfs as a function of the ratio of their stellar mass, M_* to their pre-infall halo mass, M_{200}. Now the anticorrelation between star formation and the central DM density is explicit: dwarfs with higher M_*/M_{200} have lower $\rho_{\rm DM}(150\,{\rm pc})$. This is in excellent agreement with models in which DM is heated up by bursty star formation. Several works in the literature, using different numerical techniques and different 'subgrid' star formation recipes, predicted that DM cusp–core transformations should become inefficient[8] for $M_*/M_{200} \lesssim 5\times10^{-4}$ (Peñarrubia et al. 2012; Di Cintio et al. 2014a; Chan et al. 2015; Tollet et al. 2016, and for a review see Bullock & Boylan-Kolchin 2017). This is marked by the vertical dashed line on Fig. 5 (right-hand panel). Notice, further, that this line delineates dwarfs that have extended star formation (blue) from those with only old-age stars (black).

Finally, recall that for ∼500 radial velocities, GravSphere's inference of the inner logarithmic slope of the DM density profile – $\gamma_{\rm DM}(150\,{\rm pc}) \equiv {\rm d}\ln\rho_{\rm DM}/{\rm d}\ln r(150\,{\rm pc})$ – depends on our choice of priors on $\gamma_{\rm DM}$ (Read et al. 2018). For this reason, we have focused in this paper only on the amplitude of the inner DM density, $\rho_{\rm DM}(150\,{\rm pc})$ (see Section 2). None the less, for completeness we show our results for $\gamma_{\rm DM}(150\,{\rm pc})$ in Appendix D. There, we confirm that $\gamma_{\rm DM}(150\,{\rm pc})$ is sensitive to our priors on $\gamma_{\rm DM}$. However, independently of our priors on $\gamma_{\rm DM}$, we find that dwarfs with truncated star formation have *steeper* central density profiles than those with extended star formation, consistent with our results for $\rho_{\rm DM}(150\,{\rm pc})$, above.

We have shown that the scatter in $\rho_{\rm DM}(150\,{\rm pc})$ at fixed M_* (Fig. 5, left-hand panel) cannot owe to tidal stripping and shocking. Tidal effects are certainly important for some of the Milky Way dwarfs (for example the visibly disrupting Sagittarius dSph; Ibata, Gilmore & Irwin 1995). However, the sample of dSphs that we have considered in this paper are moving on relatively benign orbits around the Milky Way. Their orbits are not sufficiently radial to affect the DM density at 150 pc (e.g. Lux et al. 2010; Gaia Collaboration et al. 2018). We have shown further that the scatter cannot owe to the dwarfs inhabiting different pre-infall mass haloes. The dwarfs certainly do inhabit a range of different pre-infall halo masses (Fig. 5, middle panel). However, this is not sufficient to

[8]Note that Di Cintio et al. (2014a) actually set this boundary to be $M_*/M_{200} = 10^{-4}$. However, from their fig. 3, this corresponds to $\gamma_{\rm DM}(0.01 < r/R_{200} < 0.02) \sim -1$. At $M_*/M_{200} = 5\times10^{-4}$, most of their simulations still have $\gamma_{\rm DM}(0.01 < r/R_{200} < 0.02) \sim -0.85$, corresponding to very little cusp–core transformation.

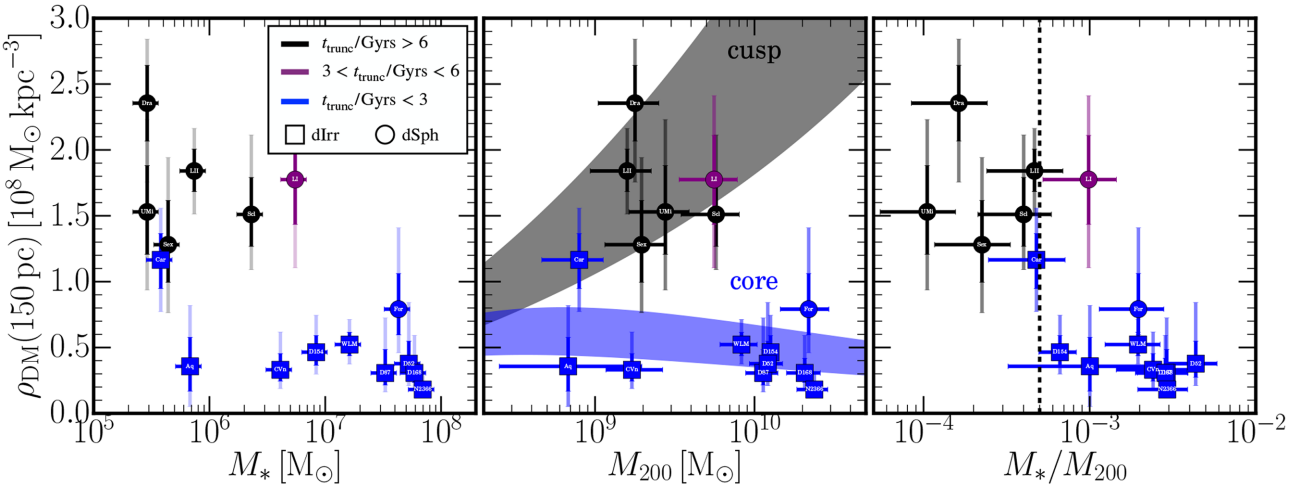

Figure 5. Left: the inner DM density of our sample of dwarfs, $\rho_{\rm DM}(150\,{\rm pc})$, as a function of their stellar masses, M_*. The blue points mark those dwarfs that stopped forming stars $t_{\rm trunc} < 3\,{\rm Gyr}$ ago; the black points those with $t_{\rm trunc} > 6\,{\rm Gyr}$; and the purple points those with $3 < t_{\rm trunc}/{\rm Gyr} < 6$ (see Table 1). The square symbols denote dIrr galaxies, whose central densities were determined from their HI rotation curves (Section 3.2); and the circle symbols denote dSph galaxies, whose central densities were determined from their stellar kinematics (Section 3.1). Notice that dwarfs with extended star formation (blue) have $\rho_{\rm DM}(150\,{\rm pc}) < 10^8\,{\rm M}_\odot\,{\rm kpc}^{-3}$, while those with only old stars (black) have $\rho_{\rm DM}(150\,{\rm pc}) > 10^8\,{\rm M}_\odot\,{\rm kpc}^{-3}$. Notice also the 'dwarf twins' – UMi, Draco, Carina, Sextans, Leo II, and Aquarius – that have similar M_* but very different $\rho_{\rm DM}(150\,{\rm pc})$. Middle: $\rho_{\rm DM}(150\,{\rm pc})$ as a function of pre-infall halo mass, M_{200}, as extrapolated from HI rotation curves (for the dIrrs) and abundance-matching (for the dSphs; see Section 4). The grey band marks the inner DM density of ΛCDM haloes assuming no cusp–core transformations take place, where the width of the band corresponds to the 1σ scatter in DM halo concentrations (equation 5). The blue band marks the same, but for the coreNFW profile from Read et al. (2016a), assuming maximal core formation. Thus, these two bands bracket the extremum cases of no cusp–core transformation and complete cusp–core transformation in ΛCDM. Notice that dwarfs with extended star formation (blue) lie along the blue track, consistent with having DM cores, while those whose star formation shut down long ago (black) lie along the grey track, consistent with having DM cusps. Right: $\rho_{\rm DM}(150\,{\rm pc})$ as a function of the stellar mass to halo mass ratio, M_*/M_{200}. Notice that dwarfs that have formed more stars as a fraction of their pre-infall halo mass have a lower central DM density. This is consistent with models in which DM is 'heated up' by repeated gas inflows and outflows driven by stellar feedback (e.g. Read & Gilmore 2005; Pontzen & Governato 2012; Di Cintio et al. 2014a; Chan et al. 2015; Tollet et al. 2016). The vertical dashed line marks the approximate M_*/M_{200} ratio below which recent models predicted that DM cusp–core transformations should become inefficient (Peñarrubia et al. 2012; Di Cintio et al. 2014a; Chan et al. 2015; Tollet et al. 2016).

explain the scatter we find in $\rho_{\rm DM}(150\,{\rm pc})$. In particular, we see no correlation between $\rho_{\rm DM}(150\,{\rm pc})$ and M_{200} (Fig. 5, middle panel). By contrast, we see a clear anticorrelation between $\rho_{\rm DM}(150\,{\rm pc})$ and the ratio M_*/M_{200} (Fig. 5, right-hand panel). This anticorrelation was predicted by models in which DM is slowly 'heated up' at the centres of dwarf galaxies by bursty star formation (Peñarrubia et al. 2012; Di Cintio et al. 2014a; Chan et al. 2015; Read et al. 2016a; Tollet et al. 2016). In Section 6, we discuss which combination of measurements would need to be wrong in order for this agreement between data and models to be spurious.

6 DISCUSSION

6.1 Comparison with previous work in the literature

6.1.1 The dwarf irregulars

Our sample of dIrrs is drawn from the Little The HI Nearby Galaxy Survey (THINGS) survey (Oh et al. 2015; Iorio et al. 2017). Oh et al. (2015) presented mass models for all of the dIrrs we discuss here, using an entirely independent derivation of their rotation curves from the raw HI datacubes. Oh et al. (2015) also favour DM cores for these dIrrs, finding an inner logarithmic slope, averaged over their full sample, of $\gamma_{\rm DM} = -0.32 \pm 0.24$. This is in excellent agreement with our findings here (see Table 1). The only dIrrs for which Oh et al. (2015) favour DM cusps are DDO 101 and DDO 210 (Aquarius). DDO 101 was discussed extensively in Read et al. (2016b). There, it was shown that DDO 101's steeply rising rotation curve could owe to an incorrect distance estimate for this dwarf. Indeed, DDO 101 did not make our final selection precisely because of its highly uncertain distance. For DDO 210, we find, similarly to Oh et al. (2015), that the uncertainties on the inner DM density and logarithmic slope are simply very large (see Table 1). In terms of the inner logarithmic slope of its DM density profile, Aquarius could indeed be cusped or cored within its 95 per cent confidence intervals (see Fig. 5). However, the *amplitude* of Aquarius' inner DM density, $\rho_{\rm DM}(150\,{\rm pc})$, is consistent with it being cored (see Fig. 5, right-hand panel).

6.1.2 The dwarf spheroidals

Among the dSphs, by far the well studied are Fornax and Sculptor, which are relatively luminous and have the largest available stellar-kinematic samples (for reviews, see Battaglia et al. 2013 and Walker 2013). While there is a general consensus that Fornax has a DM core (Goerdt et al. 2006; Walker & Peñarrubia 2011; Amorisco & Evans 2012; Cole et al. 2012; Kowalczyk et al. 2018; Pascale et al. 2018), Sculptor has proven more contentious. For example, modelling split populations using the Jeans equations and/or the Virial theorem, Battaglia et al. (2008), Agnello & Evans (2012), Walker & Peñarrubia (2011), and Amorisco & Evans (2012) all favour a central DM core; using VSPs similar to our analysis here, Richardson & Fairbairn (2014) favour a cusp; using a Schwarzschild method, split populations with axisymmetric Jeans models and a phase-space distribution function method, respectively, Breddels

et al. (2013), Zhu et al. (2016), and Strigari, Frenk & White (2017) all conclude that they cannot distinguish cusps from cores with the currently available data. Finally, Massari et al. (2017) have recently used the first internal proper motion data for Sculptor to argue that it favours a cusp. However, Strigari, Frenk & White (2018) argue that those same proper motion data are consistent with both cusps and cores.

Fig. 6 compares our new results for the cumulative DM mass profiles of Sculptor (left) and Fornax (right) to those from previous studies for which such a comparison is straightforward.[9] The grey contours show the 68 per cent (dark) and 95 per cent (light) confidence intervals of our GravSphere models. The magenta and red data points show the results from Walker & Peñarrubia (2011) and Amorisco, Agnello & Evans (2013), respectively, who both use split population methods with dynamical mass estimators to obtain measurements of the enclosed masses at different scale radii. (The light/dark error bars mark the 95 per cent and 68 per cent confidence intervals of these models, respectively.) The dashed blue curves indicate the posterior PDF that Zhu et al. (2016) obtain for a generalized DM halo model, using split populations with an axisymmetric Jeans method that includes rotation. All of these methods break the $\rho - \beta$ degeneracy (see Section 1) in different ways, while each study uses their own data selection and their own approach to determining the membership probability.

Most of the mass models for Sculptor and Fornax shown in Fig. 6 agree within their 68 per cent confidence intervals. This is remarkable given the different methodologies used to derive these mass profiles. However, a notable outlier is the Sculptor result of Walker & Peñarrubia (2011, WP11 hereafter), who report an enclosed mass at $r \sim 300$ pc that is a factor of $\sim$2 larger than that obtained in the other studies (including the present one). It is this large mass – or more precisely, the relatively steep slope required to reach this mass from WP11's more-agreeable estimate at smaller radius – that leads WP11 to conclude that Sculptor's mass profile is incompatible with an NFW cusp. WP11's methodology has been tested extensively using mock data sets drawn from equilibrium dynamical models as well as cosmological and hydrodynamical *N*-body simulations, generally supporting WP11's argument that it is the mass at *smaller* radius that is more prone to overestimation (e.g. Laporte, Walker & Peñarrubia 2013; Genina et al. 2017). However, the outer mass can be overestimated in the case of ongoing tidal heating (see the discussion by WP11) and/or departures from spherical symmetry that can conspire with unfortunate viewing angles to bias WP11's mass estimator. Even so, Genina et al. (2017) find that in just $\sim$3 per cent of their cosmologically simulated realizations of Sculptor analogs with cuspy DM haloes, the latter effect would induce sufficient systematic error to account for WP11's result.

At present, we lack a satisfactory explanation for the apparent $\sim 2\sigma$ systematic discrepancy, above. However, the key result in this paper – that we find an anti-correlation between $\rho_{\rm DM}(150\,{\rm pc})$ and M_*/M_{200} – is based on the inference of $\rho_{\rm DM}$ at 150 pc where all of the above studies agree. Furthermore, the trend exhibited across the population of dwarf galaxies in our sample should be insensitive to even large systematic errors in the mass profiles inferred for individual systems, provided that the systematic errors do not correlate with the SFH.

6.1.3 *Dark matter heating*

From the above comparisons, it is clear that the results in this paper do not owe to any special feature of our GravSphere modelling. Rather, what is new here is: (i) the comparison of the DM distribution in isolated gas-rich dwarfs with our sample of nearby gas-poor dSph; and (ii) the comparison of the inner DM density of these dwarfs with their SFHs. With a large sample of such dwarfs with excellent quality data, we are able to demonstrate that Fornax, with its extended SFH, has a shallow DM density profile similar to that of WLM and the other isolated dIrrs, while nearby dSphs that have only old-age stars are substantially denser, consistent with steeper, more cuspy, DM density profiles. These results are in good agreement with recent predictions by Bermejo-Climent et al. (2018) who used energetic arguments to show that UMi and Draco are the dSphs most likely to have a pristine DM cusps, while Fornax and Sculptor are most likely to have large DM cores. Similarly, Brook & Di Cintio (2015) used their DM heating models, combined with abundance matching, to predict DM cores in WLM and Fornax, cusps in Draco, Leo I, Leo II, and UMi, and something in-between for Sculptor and Aquarius. This is also in excellent agreement with our findings here.

Finally, the diversity of central DM densities that we find here is in good agreement with the recent study of Valli & Yu (2017). They fit an SIDM model to the classical dSphs, finding a wide range of interaction cross-sections, corresponding to a wide range of central DM densities. Similarly to our results here, they favour a low central density (high SIDM cross-section) for Fornax and a high central density (low SIDM cross-section) for Draco.[10] However, without the dIrrs to compare with, they describe Fornax (and Sextans) as 'outliers'. We favour a different interpretation. Given the good agreement between the inferred DM density profile of Fornax and that of our dIrr sample, we argue that Fornax is not an outlier, but rather a key piece of evidence for DM heating at the centres of dwarf galaxies.

6.2 Model limitations and caveats

6.2.1 *Mass modelling with stellar kinematics*

In recent years, there have been a number of studies critiquing the robustness of stellar kinematic mass modelling. The primary concerns are the effects of unmodelled triaxiality and the effect of unbound tidally stripped stars. Four recent studies have looked at the effects of triaxiality on mass modelling methods that assume spherical symmetry. Read & Steger (2017) test the GravSphere method that we use here; Laporte et al. (2013) and Genina et al. (2017) test the Walker & Peñarrubia (2011) split-population method; and Kowalczyk, Lokas & Valluri (2017) test a Schwarzschild method. All four find that triaxiality induces a small bias on the recovery that is rarely larger than the 95 per cent confidence intervals of the models. Kowalczyk et al. (2013) test the Wolf et al. (2010) Jeans mass estimators on tidally stripped mock data, finding that

[9] Previous studies that we have not included in this plot evaluate perfectly cored and/or NFW-cusped halo models separately. This makes it challenging to compare with our GravSphere models that provide a posterior probability distribution function that includes the space in between these two extremes.

[10] For the remaining dwarfs, our study and that of Valli & Yu (2017) are broadly in good agreement, though they claim tighter constraints on the central density for UMi and Sextans than our GravSphere models are able to achieve.

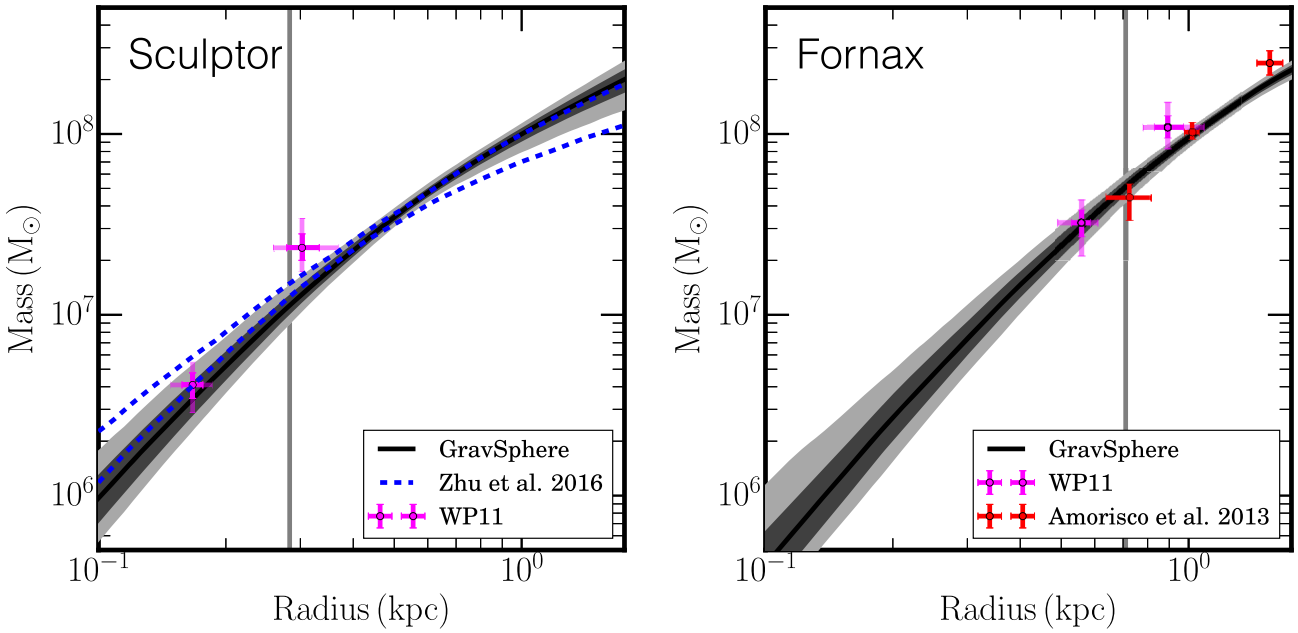

Figure 6. The cumulative DM mass profile of our GravSphere models for Sculptor (left) and Fornax (right) as compared to other determinations in the literature (see the legend). The grey contours show the 68 per cent and 95 per cent confidence intervals of our GravSphere models.

they can become significantly biased. This contrasts with our recent work in Read et al. (2018) where we show that GravSphere is able to successfully recover the radial density profile of a tidally stripped mock dwarf set-up to mimic Draco, within its 95 per cent confidence intervals. A full exploration of this difference is beyond the scope of this work, but may owe to Kowalczyk et al. (2013) using Jeans mass estimators that are more prone to bias than fully self-consistent dynamical models (e.g. Campbell et al. 2017), or to their mocks being further from dynamical equilibrium than those considered in Read et al. (2018).

6.2.2 *Mass modelling with HI rotation curves*

The list of potential pitfalls for modelling gaseous rotation curves is rather longer than for stellar kinematic mass modelling. Several studies have worried about the effects of beam smearing (e.g. Marchesini et al. 2002), non-circular motions due to a central bar (e.g. Rhee et al. 2004; Valenzuela et al. 2007), unmodelled turbulent or vertical pressure support in the disc (e.g. Valenzuela et al. 2007; Pineda et al. 2017), inclination error (e.g. Rhee et al. 2004; Read et al. 2016b), umodelled halo triaxaility (e.g. Hayashi & Navarro 2006; Kuzio de Naray & Kaufmann 2011; Oman et al. 2017), and the effect of large HI holes driven by supernovae explosions (Read et al. 2016b). In Read et al. (2016b), we explicitly tested the methodology we use here on high-resolution mock rotation curve data that include most of the above potential problems. We found that for fitted inclinations $i > 40^\circ$ (which is the case for all of the galaxies we consider in this paper), we were able to successfully recover the underlying rotation curve and obtain the correct mass distribution. The only issue that we did not explore in Read et al. (2016b) is the effect of non-circular motions due to halo triaxiality or a stellar bar. None of the galaxies in the sample we use here has a prominent stellar or gaseous bar, but they could inhabit triaxial DM haloes. Oman et al. (2017) have recently argued that this could be a significant source of bias in rotation curve modelling that typically assumes, as we have done here, a spherical DM halo. They demonstrate, using mock data from the A Project Of Simulating The Local Environment (APOSTLE) simulations, that non-circular motions due to halo triaxiality can cause DM cusps to masquerade as cores. However, the mock dwarf galaxies used in Oman et al. (2017) appear to have significantly larger non-circular motions (as determined from the residuals of their tilted ring model fits) than real galaxies in the Little THINGS survey (Oh et al. 2015; Iorio et al. 2017). Furthermore, triaxiality should induce a range of apparent inner DM logarithmic cusp slopes, with some galaxies appearing cored and others appearing cusped. This is not what we find for our sample of dIrrs that all favour a constant density DM core (see Figs 5 and A1). None the less, this is an issue that warrants more attention in future work.

6.2.3 *Systematic bias between stellar kinematic and HI rotation curve modelling*

Almost all of our high-density dwarfs are gas-free dSphs, while our low-density dwarfs are all gas-rich dIrrs. This general trend is expected if DM is heated up by bursty stellar feedback (e.g. Di Cintio et al. 2014a; Read et al. 2016a). However, the dSphs are modelled using stellar kinematics, while the dIrrs are modelled using gaseous rotation curves. Could this modelling difference be the true cause of the density dichotomy that we see here? To answer this question, it is instructive to consider two scenarios in which the results in Fig. 5 are spurious and owe to some problem with our mass modelling. In scenario A, let us suppose that all dwarfs are actually cusped, with a central density $\rho_{\rm DM}(150\,{\rm pc}) > 10^8\,{\rm M}_\odot\,{\rm kpc}^{-3}$. In this case, the following would have to be true: (i) all stellar kinematic studies to date have mismeasured Fornax's DM density profile (cf. Section 6.1); (ii) Fornax's globular clusters have found some way, as yet unknown, to survive orbiting in a dense cusped DM halo (Goerdt et al. 2006; Cole et al. 2012); (iii) the agreement between the inner DM density profile of Fornax derived using GravSphere and the dIrrs is an unfortunate coincidence (Figs 3 and A1); and (iv) all of the dIrr density profiles presented in this paper are wrong. In scenario

B, let us suppose that all dwarfs have large cores of size $\gtrsim R_{1/2}$, with central densities $\rho_{\rm DM}(150\,{\rm pc}) < 10^8\,{\rm M}_\odot\,{\rm kpc}^{-3}$. In this case: (i) the GravSphere density profiles for Draco, Sculptor, Leo I, and Leo II are wrong; (ii) the remaining dSphs must lie at the 95 per cent lower bound of their GravSphere model density profiles (Fig. 5, middle panel); and (iii) GravSphere works on mock data but fails on the real data for most dSphs. Both scenarios seem unlikely. While the results for any individual dwarf may change, it seems hard to escape the conclusion that some dwarfs have a high central DM density, while others have low central DM density.

6.2.4 *Systematic uncertainties in the pre-infall halo masses*

The results in Fig. 5 (middle and right-hand panels) rely on estimates for the pre-infall halo masses, M_{200}, of our dwarf sample. For the gas-rich dIrrs, we took these from the HI rotation curve estimates in Read et al. (2017); for the dSphs, we used the abundance matching method from Read & Erkal (2018). While both of these estimates could suffer from sizeable systematic uncertainties, such errors cannot explain the diversity of central DM densities that we find here. If we wanted all of the dwarfs to lie along the grey track in Fig. 5 (middle panel), we would have to have Fornax and all of the dIrrs inhabit haloes with masses $M_{200} < 5 \times 10^8\,{\rm M}_\odot$, inconsistent with the peak rotation curve measurements for our dIrr sample. Furthermore, we would not be able to explain how such low-mass galaxies managed to form so many stars. For these reasons, we are confident that our results are not contingent on our pre-infall halo mass estimates.

6.3 A dichotomy or a continuum of cusps and cores?

At present, our results in Fig. 5 are consistent with some dwarfs being cusped (those with only old-age stars; black), and some dwarfs being cored (those with younger stars; blue). However, as the constraints on $\rho_{\rm DM}(150\,{\rm pc})$ improve, we may find galaxies in transition between being fully cusped or fully cored. Leo I, with a star formation truncation time of $t_{\rm trunc} = 3.1\,{\rm Gyr}$, is a good candidate for such a dwarf, frozen in transition. Furthermore, we may find that the correspondence between being cusped or cored and $t_{\rm trunc}$ is not exact (see Introduction). There could be significant stochasticity in the formation of DM cores, driven by differing merger histories (e.g. Laporte & Peñarrubia 2015) and/or the spin and concentration parameters of the dwarfs' DM haloes (e.g. Read et al. 2016a). Carina is particularly interesting in this regard as it has an extended SFH, yet weakly favours a DM cusp (Fig. 5). Similarly, the 'ultrafaint' dwarfs Eridanus II and Andromeda XXV may be further examples of stochasticity, since both appear to have old-age stars and central DM cores (Amorisco 2017; Contenta et al. 2017). [Note, however, that the cores claimed in these ultrafaint dwarfs are much smaller than the $\sim$150 pc scale that we are able to probe here. As such, an alternative explanation could be that all dSphs – both classical and ultrafaint – have a small $\lesssim 100\,{\rm pc}$-size inner core that forms at high redshift, and that we are not yet able to detect yet. See Read et al. (2018) for some further discussion on this point.] We will address these questions in more detail in future work.

6.4 The Too Big to Fail problem

Several recent papers have argued that the Milky Way classical dwarfs, in the context of ΛCDM, must inhabit the most massive DM subhaloes before infall (e.g. Kim, Peter & Hargis 2017; Jethwa, Erkal & Belokurov 2018; Read & Erkal 2018). However, these massive subhaloes have central densities that are too high to be consistent with the observed stellar velocity dispersions of the Milky Way classical dwarfs (e.g. Read et al. 2006b), a problem that has become known as 'Too Big to Fail' (Boylan-Kolchin, Bullock & Kaplinghat 2011).

The nomenclature 'Too Big to Fail' (hereafter TBTF) refers to the fact that TBTF is solved if the most massive subhaloes are devoid of stars and gas, placing the classical dwarfs instead in lower mass and, therefore, lower density subhaloes. However, such a solution is puzzling because it requires the most massive subhaloes to end up dark, while their lighter cousins form stars. Such massive subhaloes ought to be 'Too Big to Fail'.

An alternative solution to TBTF is that the central density of the most massive subhaloes is lower than expected from pure DM structure formation simulations in ΛCDM (Read et al. 2006b). Indeed, Boylan-Kolchin, Bullock & Kaplinghat (2012) point out that TBTF can be cast as a 'central density problem', akin to the cusp–core problem for isolated dwarfs (see Introduction).

With the results of this paper, we are now in a position to revisit TBTF. Boylan-Kolchin et al. (2011) argue that, statistically, 2−4 of the Milky Way classical dwarfs have an unexpectedly low central density. From Fig. 5 (middle panel) of the satellite dwarfs studied here, only Fornax has a central density that is lower than expected in pure DM structure formation simulations in ΛCDM (compare the location of Fornax with the grey band on this plot). However, the Sagittarius dSph also appears to inhabit a massive pre-infall subhalo (Gibbons, Belokurov & Evans 2017; Read & Erkal 2018). If Fornax and Sagittarius inhabit massive pre-infall haloes (with $M_{200} > 10^{10}\,{\rm M}_\odot$), then this is already sufficient to significantly alleviate the Milky Way's TBTF problem. However, in addition to Fornax and Sagittarius, there may have been other Fornax-like galaxies that fell in late and did not survive. As discussed in Read et al. (2016a), early infalling dwarfs have their star formation shut down before they can fully transform their cusp to a core. Indeed, as we have shown in this paper, the Milky Way dSphs with only old-age stars are consistent with this (see Fig. 5, middle panel, black data points). By contrast, late infalling dwarfs have time to transform their cusps to cores, becoming more susceptible to tidal destruction than expected in pure DM structure formation simulations. A full solution to TBTF may require some of these late infalling cored dwarfs to be tidally destroyed (e.g. Zolotov et al. 2012; Brooks & Zolotov 2014; Wetzel et al. 2016). We will study this in more detail in future work.

6.5 The nature of DM

Our GravSphere models favour a wide range of central DM densities in dwarfs with similar M_* (Fig. 5, left-hand panel). Furthermore, the densest dwarfs are those whose star formation shut down long ago, while the low-density dwarfs have more extended star formation. These results are in excellent agreement with models in which cold DM 'heats up' at the centres of dwarf galaxies due to bursty star formation (Fig. 5, middle and right-hand panels). However, they are challenging to understand in models where large DM cores are ubiquitous. Many modifications to the nature of DM have been proposed to explain the observed DM cores in dIrr galaxies (see Introduction). However, these typically produce DM cores in *all* dwarfs, which is not what we find here. In a companion paper, we used our densest dwarf, Draco, to place a new constraint on the DM self-interaction cross-section (Read et al. 2018); dense

dwarfs like Draco can now be used to place similar constraints on any model that produces ubiquitous DM cores (e.g. ultralight axion DM; Marsh & Pop 2015; González-Morales et al. 2017).

7 CONCLUSIONS

We have used stellar kinematics and HI rotation curves to infer the radial DM density profile of eight dSph and eight dIrr galaxies with a wide range of SFHs. Our key findings are as follows:

(i) The dwarfs fell into two distinct classes. Galaxies with only old stars (>6 Gyr old) had central DM densities, $\rho_{\rm DM}(150\,{\rm pc}) > 10^8\,{\rm M}_\odot\,{\rm kpc}^{-3}$, consistent with DM cusps; those with star formation until at least 3 Gyr ago had $\rho_{\rm DM}(150\,{\rm pc}) < 10^8\,{\rm M}_\odot\,{\rm kpc}^{-3}$, consistent with DM cores (Fig. 5, left-hand panel).

(ii) We estimated pre-infall halo masses for our sample of dwarfs, using HI rotation curve measurements for the dIrr sample and abundance matching for the dSph sample. With this, we showed that their $\rho_{\rm DM}(150\,{\rm pc})$ as a function of M_{200} is in good agreement with models in which DM is kinematically 'heated up' by bursty star formation. The dwarfs with only old-age stars lay along the track predicted by the NFW profile in ΛCDM, consistent with having undergone no measurable DM heating. By contrast, those with extended star formation lay along the track predicted by the coreNFW profile from Read et al. (2016a), consistent with maximal DM heating (Fig. 5, middle panel).

(iii) We found that $\rho_{\rm DM}(150\,{\rm pc})$ for our sample of dwarfs is anticorrelated with their stellar mass to pre-infall halo mass ratio, M_*/M_{200} (Fig. 5, right-hand panel). This is also in good quantitative agreement with predictions from recent DM heating models (Peñarrubia et al. 2012; Di Cintio et al. 2014a; Chan et al. 2015; Read et al. 2016a; Tollet et al. 2016).

(iv) While not the main focus on this paper, in Appendix B we discussed the implications of our results for 'alternative gravity' models for DM. There, we showed that the dwarf 'twins' Draco and Carina provide a particularly clean test of such models. These two dwarfs have similar M_*, $R_{1/2}$, and orbit around the Milky Way, yet favour very different DM density profiles. In ΛCDM, this is explained by Carina and Draco inhabiting haloes with different pre-infall masses and concentrations (Fig. 5, middle panel). In alternative gravity theories, however, the existence of visibly similar galaxies with different gravitational force fields represents a major challenge (Fig. B1).

ACKNOWLEDGEMENTS

We would like to thank Arianna Di Cintio, Stacy McGaugh, Simon White, and Hosein Haghi for useful feedback on an early draft of this paper. We would like to thank the referee, Andrew Pontzen, for a constructive report that improved the clarity of the paper. We would also like to thank N. McMonigal for kindly providing the photometric data for Carina from McMonigal et al. (2014). JIR would like to thank the KITP in Santa Barbara and the organizers of the 'The Small-Scale Structure of Cold(?) Dark Matter' programme. This paper benefitted from helpful discussions that were had during that meeting. JIR would like to acknowledge support from SNF grant PP00P2_128540/1, STFC consolidated grant ST/M000990/1, and the MERAC foundation. This research was supported in part by the National Science Foundation under Grant No. NSF PHY-1748958. MGW is supported by National Science Foundation grant AST-1412999.

The Pan-STARRS1 Surveys (PS1) and the PS1 public science archive have been made possible through contributions by the Institute for Astronomy, the University of Hawaii, the Pan-STARRS Project Office, the Max-Planck Society and its participating institutes, the Max Planck Institute for Astronomy, Heidelberg, and the Max Planck Institute for Extraterrestrial Physics, Garching, The Johns Hopkins University, Durham University, the University of Edinburgh, the Queen's University Belfast, the Harvard-Smithsonian Center for Astrophysics, the Las Cumbres Observatory Global Telescope Network Incorporated, the National Central University of Taiwan, the Space Telescope Science Institute, the National Aeronautics and Space Administration under Grant No. NNX08AR22G issued through the Planetary Science Division of the NASA Science Mission Directorate, the National Science Foundation Grant No. AST-1238877, the University of Maryland, Eotvos Lorand University, the Los Alamos National Laboratory, and the Gordon and Betty Moore Foundation.

REFERENCES

Agnello A., Evans N. W., 2012, ApJ, 754, L39
Alexander S. G., Walentosky M. J., Messinger J., Staron A., Blankartz B., Clark T., 2017, ApJ, 835, 233
Allaert F., Gentile G., Baes M., 2017, A&A, 605, A55
Amorisco N. C., 2017, ApJ, 844, 64
Amorisco N. C., Evans N. W., 2012, MNRAS, 419, 184
Amorisco N. C., Agnello A., Evans N. W., 2013, MNRAS, 429, L89
Angus G. W., 2008, MNRAS, 387, 1481
Angus G. W., Gentile G., Diaferio A., Famaey B., van der Heyden K. J., 2014, MNRAS, 440, 746
Aparicio A., Carrera R., Martínez-Delgado D., 2001, AJ, 122, 2524
Avila-Reese V., Colín P., Valenzuela O., D'Onghia E., Firmani C., 2001, ApJ, 559, 516
Battaglia G., Helmi A., Tolstoy E., Irwin M., Hill V., Jablonka P., 2008, ApJ, 681, L13
Battaglia G., Helmi A., Breddels M., 2013, New Astron. Rev., 57, 52
Baur J., Palanque-Delabrouille N., Yèche C., Magneville C., Viel M., 2016, J. Cosmol. Astropart. Phys., 8, 012
Bekenstein J. D., 2004, Phys. Rev. D, 70, 083509
Bermejo-Climent J. R. et al., 2018, MNRAS, 479, 1514
Binney J., Mamon G. A., 1982, MNRAS, 200, 361
Binney J., Tremaine S., 2008, Galactic Dynamics. Princeton Univ. Press, Princeton, NJ, p. 747
Bode P., Ostriker J. P., Turok N., 2001, ApJ, 556, 93
Boylan-Kolchin M., Bullock J. S., Kaplinghat M., 2011, MNRAS, 415, L40
Boylan-Kolchin M., Bullock J. S., Kaplinghat M., 2012, MNRAS, 422, 1203
Brada R., Milgrom M., 2000, ApJ, 541, 556
Breddels M. A., Helmi A., van den Bosch R. C. E., van de Ven G., Battaglia G., 2013, MNRAS, 433, 3173
Brooks A. M., Zolotov A., 2014, ApJ, 786, 87
Brook C. B., Di Cintio A., 2015, MNRAS, 450, 3920
Bullock J. S., Boylan-Kolchin M., 2017, ARA&A, 55, 343
Caldwell N. et al., 2017, ApJ, 839, 20
Campbell D. J. R. et al., 2017, MNRAS, 469, 2335
Carrera R., Aparicio A., Martínez-Delgado D., Alonso-García J., 2002, AJ, 123, 3199
Chan T. K., Kereš D., Oñorbe J., Hopkins P. F., Muratov A. L., Faucher-Giguère C.-A., Quataert E., 2015, MNRAS, 454, 2981
Clowe D., Bradač M., Gonzalez A. H., Markevitch M., Randall S. W., Jones C., Zaritsky D., 2006, ApJ, 648, L109
Cole A. A., Weisz D. R., Dolphin A. E., Skillman E. D., McConnachie A. W., Brooks A. M., Leaman R., 2014, ApJ, 795, 54
Cole D. R., Dehnen W., Wilkinson M. I., 2011, MNRAS, 416, 1118

Cole D. R., Dehnen W., Read J. I., Wilkinson M. I., 2012, MNRAS, 426, 601
Contenta F. et al., 2017, MNRAS, 476, 3124
Dalcanton J. J., Hogan C. J., 2001, ApJ, 561, 35
Dawson K. S. et al., 2013, AJ, 145, 10
de Blok W. J. G., 2010, Adv. Astron., 2010, 789293
de Boer T. J. L. et al., 2012a, A&A, 539, A103
de Boer T. J. L. et al., 2012b, A&A, 544, A73
de Boer T. J. L., Tolstoy E., Lemasle B., Saha A., Olszewski E. W., Mateo M., Irwin M. J., Battaglia G., 2014, A&A, 572, A10
Del Popolo A., 2009, ApJ, 698, 2093
Del Popolo A., Pace F., 2016, Ap&SS, 361, 162
Derakhshani K., Haghi H., 2014, ApJ, 785, 166
Di Cintio A., Brook C. B., Macciò A. V., Stinson G. S., Knebe A., Dutton A. A., Wadsley J., 2014a, MNRAS, 437, 415
Di Cintio A., Brook C. B., Dutton A. A., Macciò A. V., Stinson G. S., Knebe A., 2014b, MNRAS, 441, 2986
Di Cintio A., Brook C. B., Dutton A. A., Macciò A. V., Obreja A., Dekel A., 2017, MNRAS, 466, L1
Dodelson S., 2011, Int. J. Mod. Phys. D, 20, 2749
Dohm-Palmer R. C. et al., 1998, AJ, 116, 1227
Dohm-Palmer R. C., Skillman E. D., Mateo M., Saha A., Dolphin A., Tolstoy E., Gallagher J. S., Cole A. A., 2002, AJ, 123, 813
Dolphin A. E., 2000, ApJ, 531, 804
Dolphin A. E., 2002, MNRAS, 332, 91
Dotter A., Chaboyer B., Jevremović D., Kostov V., Baron E., Ferguson J. W., 2008, ApJS, 178, 89
Dubinski J., Carlberg R. G., 1991, ApJ, 378, 496
Dutton A. A., Macciò A. V., 2014, MNRAS, 441, 3359
El-Badry K., Wetzel A., Geha M., Hopkins P. F., Kereš D., Chan T. K., Faucher-Giguère C.-A., 2016, ApJ, 820, 131
El-Zant A., Shlosman I., Hoffman Y., 2001, ApJ, 560, 636
Elbert O. D., Bullock J. S., Garrison-Kimmel S., Rocha M., Oñorbe J., Peter A. H. G., 2015, MNRAS, 453, 29
Famaey B., McGaugh S. S., 2012, Living Rev. Relativ., 15, 10
Farrow D. J. et al., 2014, MNRAS, 437, 748
Flewelling H. A. et al., 2016, preprint(arXiv:1612.05243)
Flores R. A., Primack J. R., 1994, ApJ, 427, L1
Foreman-Mackey D., Hogg D. W., Lang D., Goodman J., 2013, PASP, 125, 306
Gaia Collaboration et al., 2018, A&A, 616, A12
Gallart C. et al., 2015, ApJ, 811, L18
Gatto A., Fraternali F., Read J. I., Marinacci F., Lux H., Walch S., 2013, MNRAS, 433, 2749
Genina A. et al., 2017, MNARS, 474, 1398
Gerhard O. E., Spergel D. N., 1992, ApJ, 397, 38
Gibbons S. L. J., Belokurov V., Evans N. W., 2017, MNRAS, 464, 794
Gnedin O. Y., Zhao H., 2002, MNRAS, 333, 299
Goerdt T., Moore B., Read J. I., Stadel J., Zemp M., 2006, MNRAS, 368, 1073
Goerdt T., Moore B., Read J. I., Stadel J., 2010, ApJ, 725, 1707
González-Morales A. X., Marsh D. J. E., Peñarrubia J., Ureña-López L. A., 2017, MNRAS, 472, 1346
Hague P. R., Wilkinson M. I., 2013, MNRAS, 433, 2314
Hayashi E., Navarro J. F., 2006, MNRAS, 373, 1117
Hayashi E., Navarro J. F., Taylor J. E., Stadel J., Quinn T., 2003, ApJ, 584, 541
Hogan C. J., Dalcanton J. J., 2000, Phys. Rev. D, 62, 063511
Hu W., Barkana R., Gruzinov A., 2000, Phys. Rev. Lett., 85, 1158
Hui L., Ostriker J. P., Tremaine S., Witten E., 2017, Phys. Rev. D, 95, 043541
Ibata R. A., Gilmore G., Irwin M. J., 1995, MNRAS, 277, 781
Iorio G., Fraternali F., Nipoti C., Di Teodoro E., Read J. I., Battaglia G., 2017, MNRAS, 466, 4159
Jeans J. H., 1922, MNRAS, 82, 122
Jethwa P., Erkal D., Belokurov V., 2018, MNRAS, 473, 2060
Kaplinghat M., Tulin S., Yu H.-B., 2016, Phys. Rev. Lett., 116, 041302
Kauffmann G., 2014, MNRAS, 441, 2717
Kazantzidis S., Mayer L., Mastropietro C., Diemand J., Stadel J., Moore B., 2004, ApJ, 608, 663
Khoury J., 2015, Phys. Rev. D, 91, 024022
Khoury J., 2016, Phys. Rev. D, 93, 103533
Kim S. Y., Peter A. H. G., Hargis J. R., 2018, Phys. Rev. Lett., 121, 211302
Kirby E. N., Bullock J. S., Boylan-Kolchin M., Kaplinghat M., Cohen J. G., 2014, MNRAS, 439, 1015
Kleyna J. T., Wilkinson M. I., Evans N. W., Gilmore G., 2001, ApJ, 563, L115
Koposov S. E., Irwin M., Belokurov V., Gonzalez-Solares E., Yoldas A. K., Lewis J., Metcalfe N., Shanks T., 2014, MNRAS, 442, L85
Kowalczyk K., Łokas E. L., Kazantzidis S., Mayer L., 2013, MNRAS, 431, 2796
Kowalczyk K., Lokas E. L., Valluri M., 2017, MNRAS, 476, 2918
Kowalczyk K., del Pino A., Lokas E. L., Valluri M., 2018, MNRAS, 482, 5241
Kravtsov A. V., 2013, ApJ, 764, L31
Kuzio de Naray R., Kaufmann T., 2011, MNRAS, 414, 3617
Laporte C. F. P., Peñarrubia J., 2015, MNRAS, 449, L90
Laporte C. F. P., Walker M. G., Peñarrubia J., 2013, MNRAS, 433, L54
Leaman R. et al., 2012, ApJ, 750, 33
Lee M. G., Yuk I.-S., Park H. S., Harris J., Zaritsky D., 2009, ApJ, 703, 692
Lelli F., McGaugh S. S., Schombert J. M., Pawlowski M. S., 2017, ApJ, 836, 152
Li B., Zhao H., 2009, Phys. Rev. D, 80, 064007
Lovell M. R., Frenk C. S., Eke V. R., Jenkins A., Gao L., Theuns T., 2014, MNRAS, 439, 300
Lux H., Read J. I., Lake G., 2010, MNRAS, 406, 2312
Macciò A. V., Paduroiu S., Anderhalden D., Schneider A., Moore B., 2012, MNRAS, 424, 1105
Mamon G. A., Łokas E. L., 2005, MNRAS, 362, 95
Marchesini D., D'Onghia E., Chincarini G., Firmani C., Conconi P., Molinari E., Zacchei A., 2002, ApJ, 575, 801
Marsh D. J. E., Pop A.-R., 2015, MNRAS, 451, 2479
Mashchenko S., Wadsley J., Couchman H. M. P., 2008, Science, 319, 174
Massari D., Breddels M. A., Helmi A., Posti L., Brown A. G. A., Tolstoy E., 2017, Nat. Astron., 2, 156
Mateo M., Olszewski E. W., Walker M. G., 2008, ApJ, 675, 201
McConnachie A. W., 2012, AJ, 144, 4
McGaugh S., Milgrom M., 2013, ApJ, 775, 139
McGaugh S. S., Wolf J., 2010, ApJ, 722, 248
McMillan P. J., 2017, MNRAS, 465, 76
McMonigal B. et al., 2014, MNRAS, 444, 3139
Merrifield M. R., Kent S. M., 1990, AJ, 99, 1548
Milgrom M., 1983, ApJ, 270, 365
Moore B., 1994, Nature, 370, 629
Muñoz R. R. et al., 2006, ApJ, 649, 201
Natarajan P., Zhao H., 2008, MNRAS, 389, 250
Navarro J. F., Eke V. R., Frenk C. S., 1996a, MNRAS, 283, L72
Navarro J. F., Frenk C. S., White S. D. M., 1996b, ApJ, 462, 563
Nipoti C., Binney J., 2015, MNRAS, 446, 1820
Oh S.-H. et al., 2015, AJ, 149, 180
Oman K. A., Marasco A., Navarro J. F., Frenk C. S., Schaye J., Benítez-Llambay A., 2017, MNRAS, 482, 821
Oñorbe J., Boylan-Kolchin M., Bullock J. S., Hopkins P. F., Kereš D., Faucher-Giguère C.-A., Quataert E., Murray N., 2015, MNRAS, 454, 2092
Pascale R., Posti L., Nipoti C., Binney J., 2018, MNRAS, 480, 927
Peebles P. J. E., 2000, ApJ, 534, L127
Peñarrubia J., Navarro J. F., McConnachie A. W., 2008, ApJ, 673, 226
Peñarrubia J., Pontzen A., Walker M. G., Koposov S. E., 2012, ApJ, 759, L42
Pineda J. C. B., Hayward C. C., Springel V., Mendes de Oliveira C., 2017, MNRAS, 466, 63
Planck Collaboration et al., 2014, A&A, 571, A16
Pontzen A., Governato F., 2012, MNRAS, 421, 3464

Pontzen A., Governato F., 2014, Nature, 506, 171
Read J. I., Erkal D., 2018, preprint(arXiv:1807.07093)
Read J. I., Gilmore G., 2005, MNRAS, 356, 107
Read J. I., Steger P., 2017, MNRAS, 471, 4541
Read J. I., Wilkinson M. I., Evans N. W., Gilmore G., Kleyna J. T., 2006a, MNRAS, 366, 429
Read J. I., Wilkinson M. I., Evans N. W., Gilmore G., Kleyna J. T., 2006b, MNRAS, 367, 387
Read J. I., Agertz O., Collins M. L. M., 2016a, MNRAS, 459, 2573
Read J. I., Iorio G., Agertz O., Fraternali F., 2016b, MNRAS, 462, 3628
Read J. I., Iorio G., Agertz O., Fraternali F., 2017, MNRAS, 467, 2019
Read J. I., Walker M. G., Steger P., 2018, MNRAS, 481, 860
Rhee G., Valenzuela O., Klypin A., Holtzman J., Moorthy B., 2004, ApJ, 617, 1059
Richardson T., Fairbairn M., 2014, MNRAS, 441, 1584
Robles V. H. et al., 2017, MNRAS, 472, 2945
Rocha M., Peter A. H. G., Bullock J. S., Kaplinghat M., Garrison-Kimmel S., Oñorbe J., Moustakas L. A., 2013, MNRAS, 430, 81
Rojas-Niño A., Read J. I., Aguilar L., Delorme M., 2016, MNRAS, 459, 3349
Sánchez-Salcedo F. J., Hernandez X., 2007, ApJ, 667, 878
Schive H.-Y., Chiueh T., Broadhurst T., 2014, Nat. Phys., 10, 496
Schneider A., Trujillo-Gomez S., Papastergis E., Reed D. S., Lake G., 2017, MNRAS, 470, 1542
Shao S., Gao L., Theuns T., Frenk C. S., 2013, MNRAS, 430, 2346
Skordis C., Mota D. F., Ferreira P. G., Bœhm C., 2006, Phys. Rev. Lett., 96, 011301
Sparre M., Hayward C. C., Feldmann R., Faucher-Giguère C.-A., Muratov A. L., Kereš D., Hopkins P. F., 2017, MNRAS, 466, 88
Spencer M. E., Mateo M., Walker M. G., Olszewski E. W., 2017, ApJ, 836, 202
Spencer M. E., Mateo M., Olszewski E. W., Walker M. G., McConnachie A. W., Kirby E. N., 2018, AJ, 156, 257
Spergel D. N., Steinhardt P. J., 2000, Phys. Rev. Lett., 84, 3760
Springel V., Frenk C. S., White S. D. M., 2006, Nature, 440, 1137
Strigari L. E., Frenk C. S., White S. D. M., 2017, ApJ, 838, 123
Strigari L. E., Frenk C. S., White S. D. M., 2018, ApJ, 860, 56
Teyssier R., Pontzen A., Dubois Y., Read J. I., 2013, MNRAS, 429, 3068
Tollet E. et al., 2016, MNRAS, 456, 3542
Valenzuela O., Rhee G., Klypin A., Governato F., Stinson G., Quinn T., Wadsley J., 2007, ApJ, 657, 773
Valli M., Yu H.-B., 2017, Nat. Astron., 2, 907
van der Marel R. P., 1994, MNRAS, 270, 271
Verlinde E. P., 2016, SciPost Phys., 2, 016
Vogelsberger M., Zavala J., Loeb A., 2012, MNRAS, 423, 3740
Walker M., 2013, Dark Matter in the Galactic Dwarf Spheroidal Satellites. Springer, Berlin, p. 1039
Walker M. G., Peñarrubia J., 2011, ApJ, 742, 20, WP11
Walker M. G., Mateo M., Olszewski E. W., 2009, AJ, 137, 3100
Walker M. G., Olszewski E. W., Mateo M., 2015, MNRAS, 448, 2717
Wang W., White S. D. M., Mandelbaum R., Henriques B., Anderson M. E., Han J., 2016, MNRAS, 456, 2301
Wetzel A. R., Hopkins P. F., Kim J.-h., Faucher-Giguère C.-A., Kereš D., Quataert E., 2016, ApJ, 827, L23
Wheeler C. et al., 2017, MNRAS, 465, 2420
Wolf J., Martinez G. D., Bullock J. S., Kaplinghat M., Geha M., Muñoz R. R., Simon J. D., Avedo F. F., 2010, MNRAS, 406, 1220
Wright A. C., Brooks A. M., Weisz D. R., Christensen C. R., 2019, MNRAS, 482, 1176
Young L. M., Skillman E. D., Weisz D. R., Dolphin A. E., 2007, ApJ, 659, 331
Zhang H.-X., Hunter D. A., Elmegreen B. G., Gao Y., Schruba A., 2012, AJ, 143, 47
Zhu L., van de Ven G., Watkins L. L., Posti L., 2016, MNRAS, 463, 1117
Zolotov A. et al., 2012, ApJ, 761, 71

APPENDIX A: DM DENSITY PROFILES OF THE DWARF IRREGULAR GALAXIES

In this appendix, we show the DM density profile results for the remainder of our dIrr sample (Fig. A1). These dIrrs are all actively forming stars today (Zhang et al. 2012), but do not have SFHs measured from deep colour–magnitude diagrams (see Section 4). Notice that all of them are consistent with having constant density DM cores inside ∼500 pc. Even those that permit steeper profiles within their 95 per cent confidence intervals (e.g. CVnIdwA and DDO87) have central densities that are systematically lower than all of the dSphs, except Fornax (see Figs 3–5).

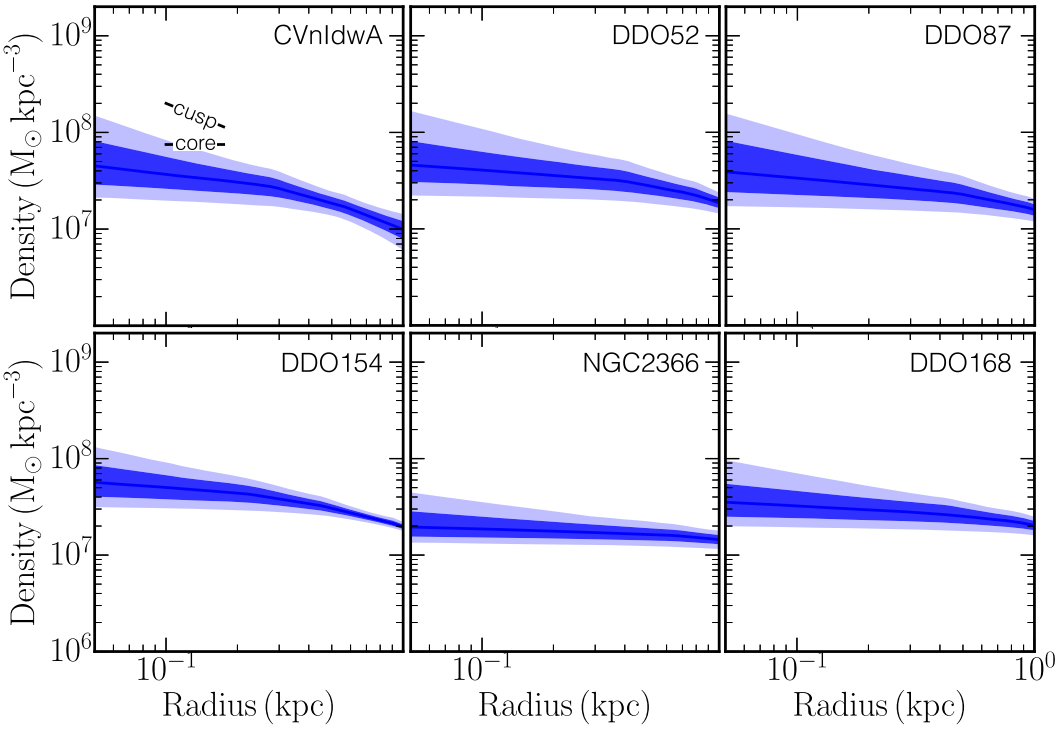

Figure A1. As Fig. 3, but for the remaining dIrrs. These galaxies have all actively been forming stars over the past 0.1 Gyr (Zhang et al. 2012), but do not have SFHs measured from deep colour–magnitude diagrams. For this reason, we show just their radial DM density profiles.

APPENDIX B: DWARF TWINS: A CHALLENGE FOR ALTERNATIVE GRAVITY THEORIES

While not the main focus of this paper, in this appendix we consider what our results imply for 'alternative gravity' theories of DM. In these theories, weak-field gravity is altered at low acceleration or on large scales to explain flat rotation curves and anomalous galactic dynamics without invoking an invisible DM (e.g. Milgrom 1983; Bekenstein 2004; Verlinde 2016).

Many of the original alternative gravity theories like MOdified Newtonian Dynamics (MOND; Milgrom 1983) and Tensor–vector–scalar gravity (TeVeS) (Bekenstein 2004) have now been ruled out as a complete explanation for DM by data from the cosmic microwave background radiation and large-scale structure (e.g. Skordis et al. 2006; Dodelson 2011), and galaxy clusters (e.g. Clowe et al. 2006; Natarajan & Zhao 2008). However, modern versions of these theories revert to a ΛCDM-like cosmology on large scales, thereby sidestepping these constraints (e.g. Li & Zhao 2009; Khoury 2015, 2016). This makes it interesting to test modifications to Newtonian gravity in the weak-field regime where alternative gravity theories have traditionally had more success (e.g. Famaey & McGaugh 2012; Lelli et al. 2017). In this Appendix, we show that the 'dwarf twins' Carina and Draco offer us a particularly clean test of such modified weak-field gravity theories.

The idea of using pairs of similar dwarfs to test modified gravity theories was first suggested by McGaugh & Milgrom (2013). They compared dwarfs with similar stellar mass and external tidal field orbiting around M31, finding that the pairs they considered were consistent with predictions in MOND. However, the orbits of the M31 dwarfs are not known, allowing some leeway in explaining pairs that do not precisely match up. By contrast, the Milky Way dwarfs Draco and Carina present a particularly clean test because of their similar stellar masses, half stellar mass radii, distances from the Milky Way[11] (Table 1), and orbits (Lux et al. 2010; Gaia Collaboration et al. 2018).

We now show quantitatively that Draco and Carina do indeed present a challenge for alternative gravity theories, using MOND as an example. Assuming spherical symmetry, the MOND force field, $\boldsymbol{g}$, relates to the standard Newtonian force field, $\boldsymbol{g}_{\rm N}$, as (e.g. Famaey & McGaugh 2012):

$$\boldsymbol{g} = \boldsymbol{g}_{\rm N} \frac{\left(1+\sqrt{1+\frac{4a_0^2}{|\boldsymbol{g}_{\rm N}|^2}}\right)^{1/2}}{\sqrt{2}} \tag{B1}$$

where $a_0 \sim 1.2 \times 10^{10}\,{\rm m\,s^{-2}}$ is the MOND acceleration scale.

Unlike Newtonian gravity, MOND is not a linear theory and so we must worry about how the force field from the Milky Way influences the dynamics of stars moving in Draco and Carina (e.g. Famaey & McGaugh 2012; Angus et al. 2014). This is called the 'external field effect'. Fortunately, these two galaxies are to a very good approximation in the 'deep MOND' regime. Using the recent

[11]Note that UMi and Sextans could also be good 'twin' candidates for Draco, however the uncertainties on their dynamical masses are larger than for Carina due to their smaller number of radial velocity measurements. Aquarius is also a promising 'twin' for Leo II, but taking into account its gas mass, its baryonic mass is actually substantially larger than Leo II's (see Table 1). Aquarius also orbits in a much weaker tidal field and may be flattened by rotation (e.g. Read et al. 2016a). For these reasons, of the dwarfs we study here, Draco and Carina are the cleanest 'twins' for testing alternative gravity models.

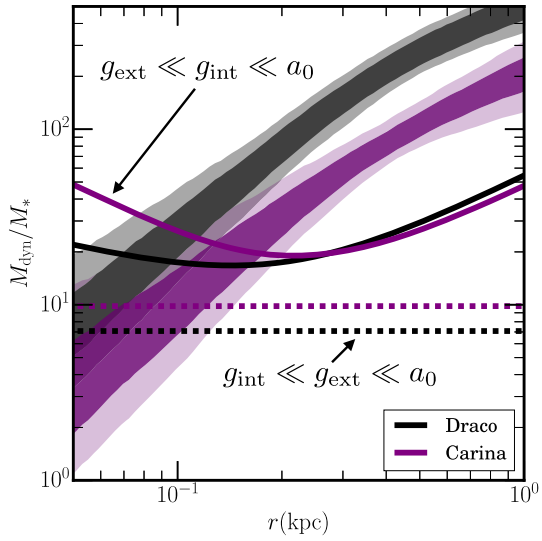

Figure B1. The dwarf 'twins' Carina and Draco: a challenge for alternative gravity explanations for DM. The contours show the 68 per cent (dark) and 95 per cent (light) confidence intervals of the ratio of the dynamical to the stellar mass, $M_{\rm dyn}/M_*$, for Draco (black) and Carina (purple), calculated from our GRAVSPHERE model chains. The solid and dashed black and purple lines show predictions for Draco and Carina in MOND in two limiting 'deep MOND' regimes, as marked (equations B1 and B2). In all cases, the MOND predictions show poor agreement with our dynamical inferences. More troublesome, however, is the similarity of the predictions for both galaxies. Their M_*, $R_{1/2}$, and distance from the Milky Way lead to similar predictions for $M_{\rm dyn}/M_*$ in MOND. Yet, their stellar kinematics imply that Draco is substantially denser than Carina. This is challenging to understand in any alternative gravity theory that seeks to fully explain DM, not just MOND.

Milky Way model from McMillan (2017),[12] the magnitude of the acceleration from the Milky Way at 100 kpc is $g_{\rm ext} \sim 10^{-11}\,{\rm m\,s^{-2}}$ which is a factor of 10 smaller than a_0. Similarly, the internal acceleration at 150 pc for Draco is $g_{\rm int} \sim 7 \times 10^{-12}\,{\rm m\,s^{-2}}$. The dynamics in this deep MOND limit then fall into two limiting cases: the 'quasi-Newtonian' regime, where $g_{\rm int} \ll g_{\rm ext} \ll a_0$; and the isolated regime, where $g_{\rm ext} \ll g_{\rm int} \ll a_0$ (e.g. Derakhshani & Haghi 2014). Carina and Draco lie closer to the quasi-Newtonian regime than the isolated regime, but we will calculate results for both to show these two extremum cases.

In the quasi-Newtonian regime, the dynamics become Newtonian but with a modified gravitational constant, $G \rightarrow Gg_{\rm ext}/a_0$ (Derakhshani & Haghi 2014). In this case, the ratio of the dynamical mass to the stellar mass becomes:

$$\frac{M_{\rm dyn}}{M_*} = \frac{g_{\rm ext}}{a_0} = {\rm const.} \tag{B2}$$

where $g_{\rm ext}$ will be slightly different for Draco and Carina due to their different distances from the Milky Way centre (see Table 1).

In the isolated regime, $|\boldsymbol{g}_{\rm N}| \ll a_0$ and from equation (B1), we obtain:

$$\frac{M_{\rm dyn}}{M_*} \simeq \sqrt{\frac{a_0}{GM_*(r)}}r \tag{B3}$$

Using the best-fitting $M_*(r)$ from the GRAVSPHERE model fits to the projected light profiles of Draco and Carina, in Fig. B1 we show predictions for $M_{\rm dyn}/M_*$ for Draco and Carina in MOND. We show results for both the isolated regime (solid lines) and the quasi-Newtonian regime (dashed lines), as marked on the figure. The contours show the 68 per cent (dark) and 95 per cent (light) confidence intervals of the ratio of the dynamical to the stellar mass, $M_{\rm dyn}/M_*$, for Draco (black) and Carina (purple) calculated from our GRAVSPHERE model chains. Notice that in all cases, the MOND predictions show poor agreement with our dynamical inferences. Indeed, it has been noted in the literature before that Draco (Gerhard & Spergel 1992; Kleyna et al. 2001; Sánchez-Salcedo & Hernandez 2007; McGaugh & Wolf 2010; Alexander et al. 2017) and Carina (Angus 2008; Alexander et al. 2017) are poorly fit by MOND, even when accounting for the external field effect and tides (Angus et al. 2014). Here, we point out an even more severe problem: these two galaxies require *different dynamical mass profiles for almost the same radial light profile*. This is a challenge not only for MOND, but for *any* weak-field gravity theory that seeks to fully explain DM.

In the context of ΛCDM, the different central densities of Carina and Draco can be understood as owing to their different pre-infall halo masses and concentrations (see Fig. 5). In alternative gravity theories, the only possible explanation is that either one or both of these galaxies is not in dynamical equilibrium. However, at least in MOND, such an explanation is problematic. Brada & Milgrom (2000) showed that Draco and Carina will be largely immune to tidal effects in MOND if their orbital pericentres are $r_{\rm p} \gtrsim 32$ and $\gtrsim 41$ kpc, respectively. The latest proper motion data from *Gaia* DR2 for these two galaxies (assuming the Milky Way 'model 2' from Gaia Collaboration et al. 2018) gives $r_{\rm p} = 32^{+6.1}_{-5.3}$ kpc for Draco and $r_{\rm p} = 74.5^{+23.7}_{-19.5}$ kpc for Carina, suggesting only a weak tidal influence from the Milky Way. Indeed, observational evidence for tides – in the form of a velocity gradient, inflated velocity dispersion at large radii and/or feature in the photometric light profile – has been reported only for Carina (Muñoz et al. 2006) and even this is contested (McMonigal et al. 2014). Finally, Angus et al. (2014) presented a detailed numerical calculation of the effect of tides on satellite galaxies in MOND. They found that tides are unable to sufficiently inflate the velocity dispersion of Carina in MOND to explain the data. While they did not explicitly model Draco, they showed that lowering the pericentre for their Carina models led to more tidal stripping, lowering the mass of Carina and, ultimately, *lowering* its velocity dispersion. It seems that, at least in MOND, it is not possible to simultaneously explain the data for Carina and Draco.

APPENDIX C: VARYING THE SCALE AT WHICH WE ESTIMATE THE INNER DM DENSITY

In this appendix, we show how our results change if we vary the scale at which we estimate the inner DM density. In Fig. C1, we show the inner DM density, $\rho_{\rm DM}(r_{\rm S})$, for $r_{\rm S} = 100$, 200, and 300 pc, as marked on the panels. The data points and contours are as in Fig. 5. As can be seen, our results are not altered by the choice of $r_{\rm S}$. For $r_{\rm S} = 100$ pc (left-hand panel), we still see a clear separation in density between those dwarfs that stopped forming stars long ago (black) and those that formed stars until recently (blue). However, the uncertainties on $\rho_{\rm DM}(100\,{\rm pc})$ are larger than for our default choice of $\rho_{\rm DM}(150\,{\rm pc})$. As $r_{\rm S}$ is increased, the error bars on $\rho_{\rm DM}(r_{\rm S})$ shrink, but so too does the difference between cusped and cored models in this space. Our default choice of $r_{\rm S} = 150$ pc represents a compromise between

[12] We calculate the enclosed mass as a function of radius for this model using the https://github.com/PaulMcMillan-Astro/GalPot code.

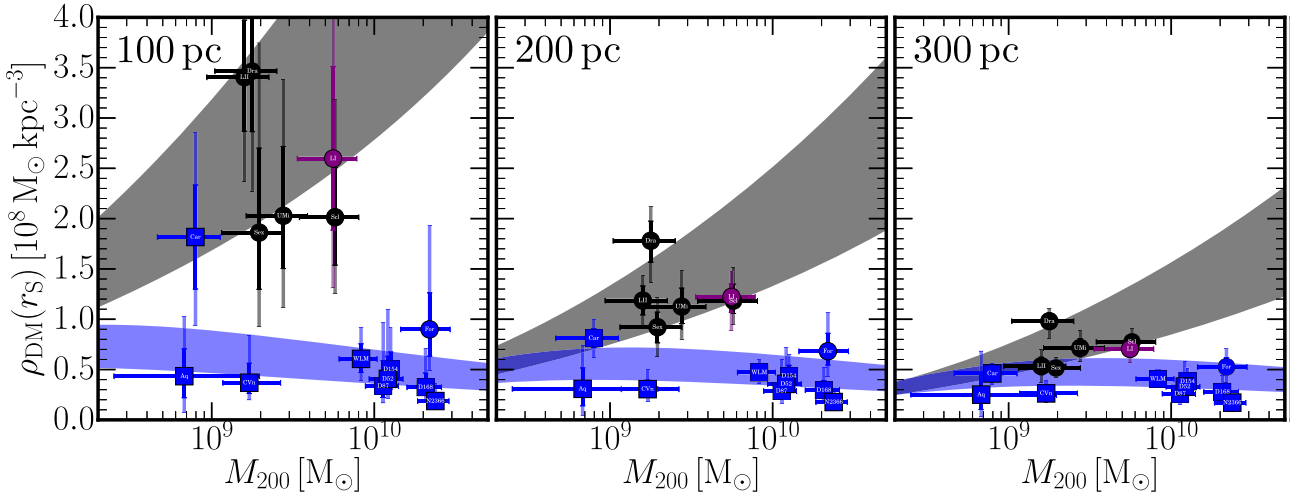

Figure C1. Varying the scale at which we estimate the inner DM density. From left to right, the panels show the inner DM density, $\rho_{\rm DM}(r_{\rm S})$, for $r_{\rm S} = 100$, 200, and 300 pc, as marked. The data points and contours are as in Fig. 5.

minimizing the error on $\rho_{\rm DM}(r_{\rm S})$ and maximizing the difference between cusped and cored models.

APPENDIX D: GRAVSPHERE CONSTRAINTS ON THE LOGARITHMIC SLOPE OF THE INNER DM DENSITY PROFILE

In this appendix, we present our GRAVSPHERE model inference of $\gamma_{\rm DM}(150\,{\rm pc})$ for our sample of dwarfs. Recall that in Read et al. (2018), we showed that $\gamma_{\rm DM}(150\,{\rm pc})$ depended on our choice of priors on $\gamma_{\rm DM}$. To show this, we introduced a rather extreme prior on $\gamma_{\rm DM}$ designed to explicitly bias our models towards cores. We assumed a flat prior over the range $-3 < \gamma'_{\rm DM} < 2$, setting $\gamma_{\rm DM} = 0$ if $\gamma'_{\rm DM} > 0$ and $\gamma_{\rm DM} = \gamma'_{\rm DM}$ otherwise. In the absence of constraining data, this 'AltGam' prior biases GRAVSPHERE towards cores by creating a large region of hypervolume in which $\gamma_{\rm DM} = 0$. (Note that we consider this prior to be extreme, using it only to test our sensitivity to priors on $\gamma_{\rm DM}$.)

In Fig. D1, we show our inference of $\gamma_{\rm DM}(150\,{\rm pc})$ for our default priors on $\gamma_{\rm DM}$ (left) and using the above AltGam prior (right). The bottom panels show the corresponding results for $\rho_{\rm DM}(150\,{\rm pc})$. Similarly to our findings in Read et al. (2018), our results for $\gamma_{\rm DM}(150\,{\rm pc})$ depend on our priors, whereas $\rho_{\rm DM}(150\,{\rm pc})$ is more robust. This is why we focus throughout this paper on our inference of $\rho_{\rm DM}(150\,{\rm pc})$ rather than $\gamma_{\rm DM}(150\,{\rm pc})$. None the less, while $\gamma_{\rm DM}(150\,{\rm pc})$ systematically shifts with our prior, the ordering of the dwarfs remains unchanged. Notice that dwarfs with old-age stars (black data points) are systematically steeper at 150 pc than those with younger stellar populations (blue data points). This is consistent with our findings for $\rho_{\rm DM}(150\,{\rm pc})$.

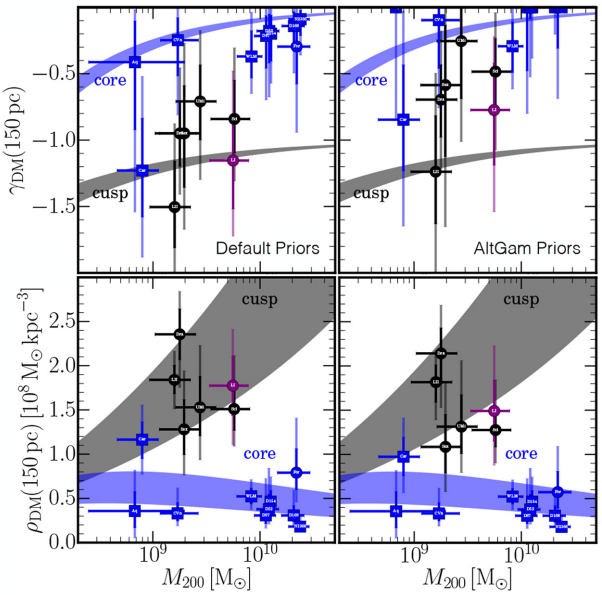

Figure D1. The central logarithmic cusp slope of the DM density profile – $\gamma_{\rm DM}(150\,{\rm pc}) \equiv {\rm d}\ln\rho_{\rm DM}/{\rm d}\ln r(150\,{\rm pc})$ – as a function of M_{200} using our default priors on $\gamma_{\rm DM}$ (top left) and using an extreme prior designed to bias our GRAVSPHERE models towards cores ('AltGam'; top right panel and see the text for details). The colour of the points is as in Fig. 5. The grey and blue bands bracket the extremum cases of no cusp–core transformation and complete cusp–core transformation in ΛCDM, respectively (cf. the similar bands in Fig. 5, middle panel). The bottom two panels show similar results for $\rho_{\rm DM}(150\,{\rm pc})$ using our default priors (left) and the AltGam priors (right). Notice that GRAVSPHERE's inference of $\gamma_{\rm DM}(150\,{\rm pc})$ is affected by the priors on $\gamma_{\rm DM}$, while its inference of $\rho_{\rm DM}(150\,{\rm pc})$ is not. However, the ordering of $\gamma_{\rm DM}(150\,{\rm pc})$ is unaffected by the priors: dwarfs that have only old-age stars (black data points) are systematically steeper than those with a younger stellar population (blue data points).

This paper has been typeset from a TEX/LATEX file prepared by the author.